



HAL
open science

Extracellular endosulfatase Sulf-2 harbors a chondroitin/dermatan sulfate chain that modulates its enzyme activity

Rana El Masri, Amal Seffouh, Caroline Roelants, Ilham Seffouh, Evelyne Gout, Julien Pérard, Fabien Dalonneau, Kazuchika Nishitsuji, Fredrik Noborn, Mahnaz Nikpour, et al.

► **To cite this version:**

Rana El Masri, Amal Seffouh, Caroline Roelants, Ilham Seffouh, Evelyne Gout, et al.. Extracellular endosulfatase Sulf-2 harbors a chondroitin/dermatan sulfate chain that modulates its enzyme activity. Cell Reports, 2022, 38 (11), pp.110516. 10.1016/j.celrep.2022.110516 . hal-03637587

HAL Id: hal-03637587

<https://hal.science/hal-03637587>

Submitted on 13 Apr 2022

HAL is a multi-disciplinary open access archive for the deposit and dissemination of scientific research documents, whether they are published or not. The documents may come from teaching and research institutions in France or abroad, or from public or private research centers.

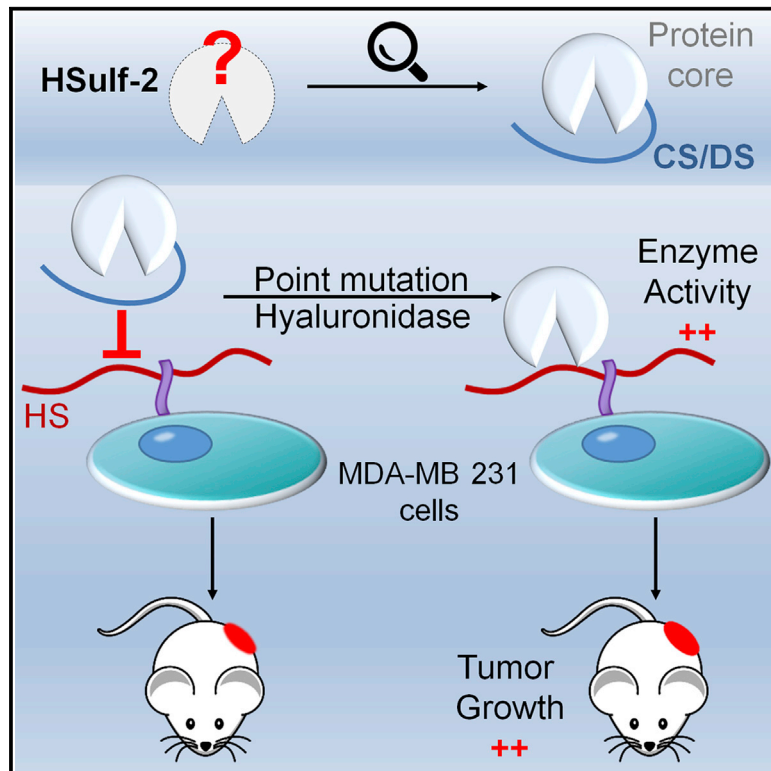
L'archive ouverte pluridisciplinaire **HAL**, est destinée au dépôt et à la diffusion de documents scientifiques de niveau recherche, publiés ou non, émanant des établissements d'enseignement et de recherche français ou étrangers, des laboratoires publics ou privés.



Distributed under a Creative Commons Attribution 4.0 International License

Extracellular endosulfatase Sulf-2 harbors a chondroitin/dermatan sulfate chain that modulates its enzyme activity

Graphical abstract



Authors

Rana El Masri, Amal Seffouh,
Caroline Roelants, ...,
Hugues Lortat-Jacob, Odile Filhol,
Romain R. Vivès

Correspondence

romain.vives@ibs.fr (R.R.V.),
odile.filhol-cochet@cea.fr (O.F.)

In brief

El Masri et al. show that human extracellular endosulfatase H sulf-2 harbors a glycosaminoglycan (GAG) chain that modulates its ability to bind and desulfate heparan sulfate and tunes its tumor-promoting properties *in vivo*. Removal of H sulf-2 GAG chain can be achieved by mammalian hyaluronidases, another class of GAG-processing enzymes.

Highlights

- Human extracellular endosulfatase H sulf-2 is a CS/DS proteoglycan
- The CS/DS chain of H sulf-2 tunes its enzyme activity
- H sulf-2 lacking the CS/DS chain displays enhanced pro-oncogenic activity
- Mammalian hyaluronidases digest H sulf-2 CS/DS chain



Article

Extracellular endosulfatase Sulf-2 harbors a chondroitin/dermatan sulfate chain that modulates its enzyme activity

Rana El Masri,^{1,8} Amal Seffouh,^{1,8} Caroline Roelants,² Ilham Seffouh,³ Evelyne Gout,¹ Julien Pérard,⁴ Fabien Dalonneau,¹ Kazuchika Nishitsuji,⁵ Fredrik Noborn,⁶ Mahnaz Nikpour,⁶ Göran Larson,⁶ Yoann Crétinon,¹ Mélanie Friedel-Arboleas,¹ Kenji Uchimura,⁷ Régis Daniel,³ Hugues Lortat-Jacob,¹ Odile Filhol,^{2,*} and Romain R. Vivès^{1,9,*}

¹Université Grenoble Alpes, CNRS, CEA, IBS, Grenoble, France

²Université Grenoble Alpes, INSERM, CEA, IRIG-Biosanté, UMR 1292, 38000 Grenoble, France

³Université Paris-Saclay, Université Evry, CNRS, LAMBE, 91025 Evry-Courcouronnes, France

⁴Université Grenoble Alpes, CNRS, IRIG – DIESE – CBM, CEA-Grenoble, 38000 Grenoble, France

⁵Department of Biochemistry, Wakayama Medical University, Wakayama 641-8509, Japan

⁶Department of Laboratory Medicine, University of Gothenburg, Sahlgrenska University Hospital, Gothenburg, Sweden

⁷Université Lille, CNRS, UMR 8576 – UGSF – Unité de Glycobiologie Structurale et Fonctionnelle, 59000 Lille, France

⁸These authors contributed equally

⁹Lead contact

*Correspondence: romain.vives@ibs.fr (R.R.V.), odile.filhol-cochet@cea.fr (O.F.)

<https://doi.org/10.1016/j.celrep.2022.110516>

SUMMARY

Sulfs represent a class of unconventional sulfatases which provide an original post-synthetic regulatory mechanism for heparan sulfate polysaccharides and are involved in multiple physiopathological processes, including cancer. However, Sulfs remain poorly characterized enzymes, with major discrepancies regarding their *in vivo* functions. Here we show that human Sulf-2 (HSulf-2) harbors a chondroitin/dermatan sulfate glycosaminoglycan (GAG) chain, attached to the enzyme substrate-binding domain. We demonstrate that this GAG chain affects enzyme/substrate recognition and tunes HSulf-2 activity *in vitro* and *in vivo*. In addition, we show that mammalian hyaluronidase acts as a promoter of HSulf-2 activity by digesting its GAG chain. In conclusion, our results highlight HSulf-2 as a proteoglycan-related enzyme and its GAG chain as a critical non-catalytic modulator of the enzyme activity. These findings contribute to clarifying the conflicting data on the activities of the Sulfs.

INTRODUCTION

Eukaryotic sulfatases have historically been defined as intracellular exoenzymes participating in the metabolism of a large array of sulfated substrates such as steroids, glycolipids, and glycosaminoglycans (GAGs) through hydrolysis of sulfate ester bonds under acidic conditions (Hanson et al., 2004). However, the field took a dramatic turn two decades ago with the discovery of the Sulfs (Dhoot et al., 2001; Morimoto-Tomita et al., 2002). Unlike all other sulfatases, Sulfs were shown to be extracellular endosulfatases that catalyzed the specific 6-O-desulfation of cell-surface and extracellular matrix heparan sulfate (HS), a polysaccharide with vast protein-binding properties and biological functions (El Masri et al., 2017; Li and Kusche-Gullberg, 2016; Sarrazin et al., 2011). Unlike all other sulfatases, Sulfs could not be related to a straightforward metabolic function but rapidly emerged as a major regulatory mechanism of HS biological activities, with roles in many physiopathological processes, including embryonic development, tissue homeostasis, and cancer (Bret et al., 2011; Rosen and Lemjabbar-Alaoui, 2010; Vives et al., 2014).

Sulfs share a common molecular organization (Figure 1). The furin-processed mature form features a general sulfatase-conserved N-terminal catalytic domain (CAT) including the enzyme active site (and, notably, the catalytic *N*-formylglycine [FGly] converted cysteine residue) and a unique highly basic hydrophilic domain (HD), which shares no homology with any other known protein and is responsible for high-affinity binding to HS substrates (Ai et al., 2006; Frese et al., 2009; Seffouh et al., 2013, 2019a; Tang and Rosen, 2009). Sulfs display a number of post-translational modifications (PTMs) (Morimoto-Tomita et al., 2002). Furin cleavage (Tang and Rosen, 2009) and *N*-glycosylations (Ambasta et al., 2007; Seffouh et al., 2019b) may be dispensable for the enzyme activity but play a role in the enzyme attachment to the cell surface, while conversion of C₈₈ into an FGly residue is a hallmark of all sulfatases and is essential for catalytic activity (Dierks et al., 2005). Recent studies reported that human Sulfs (HSulfs) catalyzed the 6-O-desulfation of HS through an original, processive, and orientated mechanism (Seffouh et al., 2013), and that substrate recognition by the enzyme HD domain involved multiple, highly dynamic, non-conventional interactions (Harder et al., 2015; Walhorn et al., 2018).



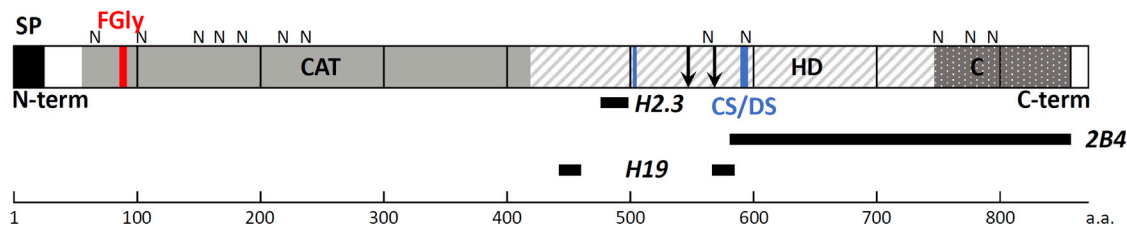


Figure 1. Schematic representation of HSulf-2 molecular organization, PTMs, and antibody epitopes

HSulf-2 870 amino acid (aa) pro-protein comprises a signal peptide (SP, black box) and a polypeptide processed through furin cleavage (black arrows) into two N-terminal (N-term) and C-terminal (C-term) subunits. HSulf-2 comprises two major functional domains: a catalytic domain (CAT, in gray) and a highly basic hydrophilic domain (HD, hatched in gray), and features a C-terminal region sharing homology with glucosamine-6-sulfatase homolog (C, dotted). Potential *N*-glycosylation sites (N), the catalytic FGly residue (FGly, in red and bold), and the SG dipeptides (blue, in bold for S₅₈₈G) and antibody epitopes (black bars) are indicated. The theoretical molecular weight (MW) of the mature HSulf-2 is 98.1 kDa; the estimated MW of the protein including *N*-glycosylation is ~125 kDa (75 and 50 kDa for the N-terminal and C-terminal subunits, respectively).

However, despite increasing interest, Sulfs remain highly elusive enzymes. Little is known about their molecular structures, catalytic mechanisms, and substrate specificities. Our limited understanding of these enzymes is well illustrated by the wealth of conflicting data in the literature, reporting major discrepancies between *in vitro* and *in vivo* data according to the biological system or the enzyme isoforms considered. This is particularly clear in cancer, where both anti-oncogenic and pro-oncogenic effects of the Sulfs have been reported (Rosen and Lemjabbar-Alaoui, 2010; Vives et al., 2014; Yang et al., 2011).

RESULTS

HSulf-2 is an enzyme modified with a CS/DS chain

Recently, we achieved high-yield expression and purification of HSulf-2, which paved the way to progress in the biochemical characterization of this enzyme (Seffouh et al., 2019a). Surprisingly, the purification step of size-exclusion chromatography (SEC) highlighted an unexpectedly high apparent molecular weight (aMW) for the enzyme (>~1,000 kDa for an expected MW of ~125 kDa) (Figure 2A), although possible protein aggregation or high-order oligomerization were ruled out by quality control negative staining electron microscopy (Seffouh et al., 2019a). Noteworthy, we also failed to detect the C-terminal chain containing the enzyme HD domain using PAGE analysis (Figure 2B, lane 1), even if the presence of both chains was ascertained by Edman N-terminal sequencing (Seffouh et al., 2019a). In line with this, we previously reported unusually weak mass spectrometry (MS) ionization efficiency of the HSulf-2 C-terminal chain (Seffouh et al., 2019b).

To clarify this unusual behavior, we analyzed HSulf-2 using different biophysical approaches, including SEC coupled to multi-angle laser light scattering (SEC-MALLS) and small-angle X-ray scattering (SAXS). SEC-MALLS is a method for measuring the absolute molecular mass and concentration of a particle in solution that is independent of its dimensions and shape. Analysis of HSulf-2 confirmed our previous observations (Figure 2D). The protein eluted as a broad peak, characterized by a high polydispersity score ($M_w/M_n = 1.322$) and a low-confidence, calculated MW of 570 ± 103 kDa. Measurement of light scattering at the center of the peak provided a more accurate measurement

of 423 ± 28.8 kDa. SAXS analysis yielded Guinier plots and pair-distribution function in accordance with a D_{max} of 40 ± 3 nm, suggesting an elongated molecular shape with an aMW of ~700 kDa, which supported our SEC-MALLS data (Figures 2E and S1A–S1D). Furthermore, results suggested the presence of two distinct domains within HSulf-2: a globular domain and an extended, flexible, probably partially unfolded region. Interestingly, similar analysis performed on an HD-devoid HSulf-2 variant (HSulf-2 Δ HD) showed only the globular domain (Figures S1I–S1L), with an 11 nm size that fitted the expected size of the CAT domain. However, it seemed unlikely that the HD domain on its own could account for the second, large flexible region.

We thus initially speculated that the enzyme could have been purified in complex with HS substrate polysaccharide chains, thus accounting for the observed elongated form. To test this, we treated HSulf-2 with heparinases (to depolymerize potentially bound HS substrate) or chondroitinase ABC (to depolymerize non-substrate GAGs of CS/DS types) prior to SEC. The results showed no effect of the heparinase treatment (Figure S2B), while digestion with chondroitinase ABC dramatically delayed HSulf-2 SEC elution time (~1 min shift), thus indicating the presence of CS/DS associated with the enzyme (Figure 2A). We therefore pre-incubated HSulf-2 with 2 M NaCl prior to the injection into the SEC column to separate the enzyme from tightly bound GAG chains (Figure S2C). Unexpectedly, this had no effect on the enzyme elution time compared with the untreated sample, thereby suggesting a possible covalent linkage between the polysaccharide and the protein. In addition, chondroitinase ABC treatment allowed for detection of a broad additional band of ~50 kDa aMW (Figure 2B). This band was assigned to the enzyme C-terminal subunit, as confirmed by western blot (WB) analysis (Figure 2B). Of note, the HSulf-2 Δ HD variant (lacking the HD but not the enzyme C-terminal region) did not exhibit such a band on PAGE (Seffouh et al., 2019a). We therefore concluded from these results that a CS/DS chain was covalently attached to the HSulf-2 HD domain. The presence of such a chain could account for the high aMW determined by SAXS and SEC, and could also hinder migration/detection of the C-terminal subunit in PAGE/WB.

GAGs are covalently bound to specific glycoproteins termed proteoglycans (PGs), through a specific attachment site involving the serine residue of an SG dipeptide starting with a

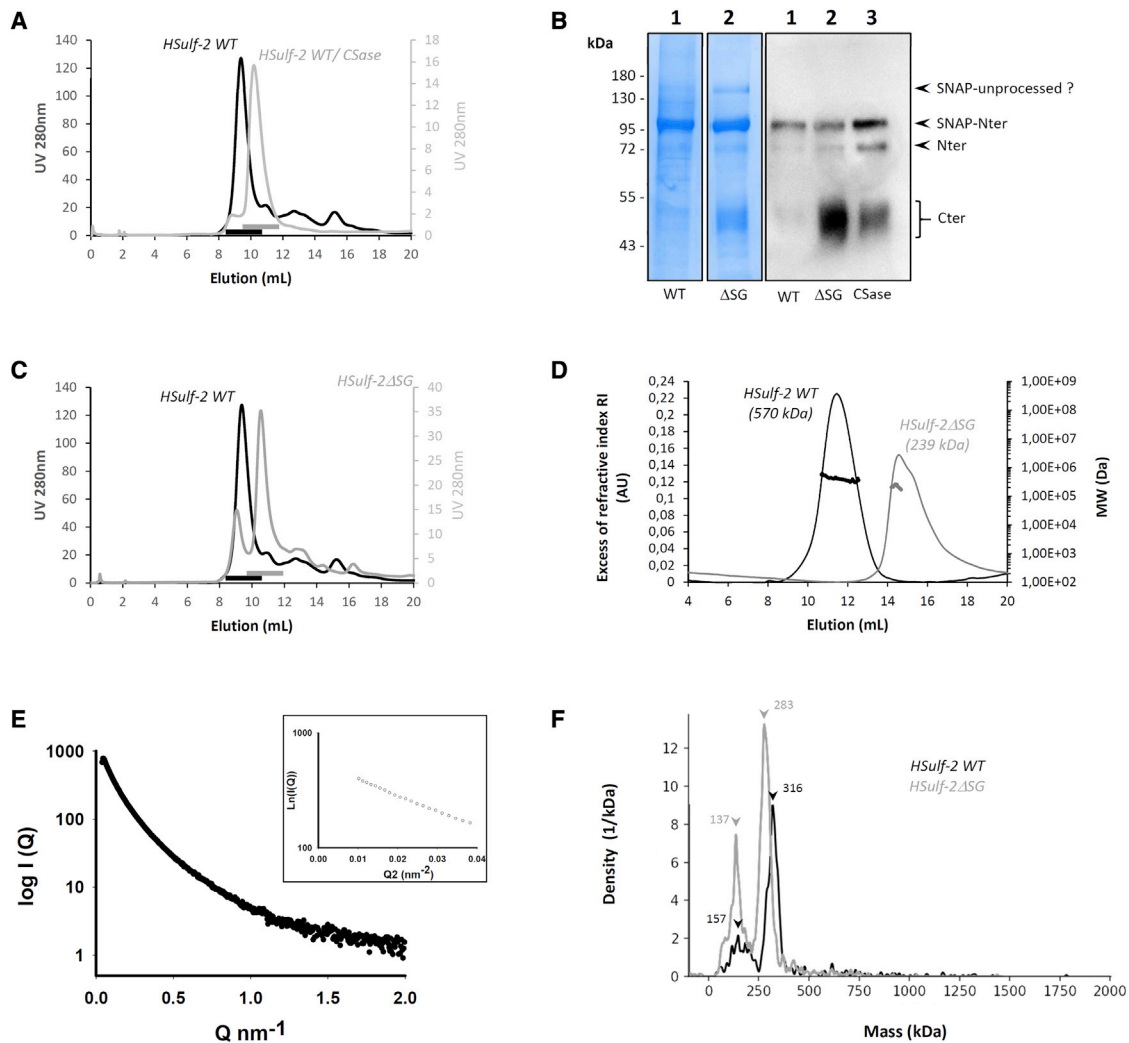


Figure 2. Purification and characterization of HSulf-2 and HSulf-2ΔSG

(A) Size-exclusion chromatography (SEC) profile of HSulf-2 WT (black) and chondroitinase ABC pre-treated HSulf-2 (gray), showing an elution time shift of ~ 1 min. Black/gray bars indicate Sulf-containing fractions.

(B) PAGE/Coomassie blue staining and western blot (WB) analysis of HSulf-2 WT (WT, lanes 1), HSulf-2ΔSG (ΔSG, lanes 2) and chondroitinase ABC pre-treated HSulf-2 (CS, lane 3), using the anti-HD H19 antibody. Analysis shows a ~ 95 kDa band corresponding to the SNAP-tag N-terminal subunit in fusion with the SNAP tag (SNAP-Nter) and multiple/broad ~ 50 kDa bands corresponding to the C-terminal subunit, which includes HSulf-2 HD domain (Cter). Of note, a residual ~ 75 kDa band corresponding to the N-terminal subunit lacking its SNAP tag could also be detected (Nter). In addition, Coomassie blue staining but not WB revealed the presence of a band, which may correspond to the full-length, unprocessed GAG-free HSulf-2 form (SNAP-unprocessed?).

(C) SEC profile of HSulf-2 WT (black) and HSulf-2ΔSG (gray), showing an elution time shift of ~ 1.2 min. Black/gray bars indicate Sulf-containing fractions.

(D) SEC-MALLS analysis of HSulf-2 WT (black) and HSulf-2ΔSG (gray).

(E) Scatter curves of experimental data determined by SAXS at room temperature for HSulf-2 WT (0.6 mg/mL) in solution. Inset shows the linear dependence of $\ln[I(Q)]$ versus Q^2 determined by Guinier plot at 0.6 mg/mL with R_g of 13 nm and I_0 of 700 with a Porod volume of more than 1,000. HSulf-2 WT gives MW_{exp} 700 kDa, MW_{malls} 570 ± 103 kDa, and MW_{th} protein 98.53 kDa. These data indicate the presence of an elongated molecule with a potential rod shape.

(F) Mass photometry analysis of HSulf-2 WT (black) and HSulf-2ΔSG (gray). Arrows show the peaks, and corresponding MWs in kDa are indicated.

xylose residue (Esko and Zhang, 1996). As such, xylosides compete with these attachment sites and strongly induce the synthesis of free GAG chains (mostly CS/DS) while inhibiting the covalent linkage of GAG on PGs (Chua and Kuberan, 2017). Whereas an increase in the synthesis of free GAG chains would promote the formation of GAG-protein non-covalent interactions, SEC analysis of HSulf-2 expressed in xyloside-treated HEK 293 cells showed a dramatic reduction of the high-amW

form and concomitant increase of a form eluting as the chondroitinase ABC-treated HSulf-2 (Figure S2D). This result thus further supports the covalent nature of the GAG chain attachment on HSulf-2. Examination of HSulf-2 amino acid sequence showed two SG dipeptides: S₅₀₈G and S₅₈₃G. We thus expressed and produced a HSulf-2 variant lacking these two motifs (HSulf-2ΔSG). The HSulf-2ΔSG variant eluted at the same time as seen in the chondroitinase ABC-treated wild-type (WT) HSulf-2

(~1.2 min shift compared with WT, Figure 2C), with restored detection of the C-terminal chain by Coomassie blue-stained PAGE and WB analysis (Figure 2B). Both SG dipeptides are located within the enzyme HD domain, but on each side of the furin cleavage sites (Figure 1). As our PAGE/WB data located the CS/DS chain on the C-terminal subunit, we thus speculated that the S₅₈₃G motif downstream of the furin cleavage sites was the actual GAG attachment site on HSulf-2. To assess this, we performed single mutations of the first and second sites. Size-exclusion analysis of the resulting variants validated the presence of a CS/DS-type GAG chain on the S₅₈₃G, but not S₅₀₈G, dipeptide motif (Figures S2E and S2F). Finally, we also confirmed that the presence of N- and C-terminal tags did not bias the results, as tobacco etch virus protease digestion did not affect SEC elution times of HSulf-2 WT, chondroitinase ABC-treated HSulf-2 WT, or HSulf-2ΔSG (Figure S3).

To provide further evidence of the presence of a GAG chain on HSulf-2, we analyzed HSulf-2ΔSG variant by MS. Matrix-assisted laser desorption/ionization time-of-flight (MALDI-TOF) MS analysis of HSulf-2ΔSG showed a major peak at *m/z* 53,885 that we assigned to the doubly charged ion [M + 2H]²⁺ of the whole HSulf-2 variant. Interestingly, corresponding mono- and triple-charged ions at *m/z* 108,250 and 37,180 were also observed. Based on this distribution of multiple charged ions, an average experimental mass value of 108,388 ± 506 g mol⁻¹ was determined for the whole HSulf-2ΔSG. HSulf-2ΔSG thus exhibited a ~25 kDa lower average mass value compared with HSulf-2 WT average MW previously determined by MALDI MS (133.115 kDa) (Seffouh et al., 2019b). Such mass difference likely corresponds to mass contribution of the GAG chain that could comprise as much as ~60 disaccharides (Figure S4). In addition, we used a strategy originally designed to identify new proteoglycans (Noborn et al., 2015). Nano-scale liquid chromatography-tandem MS (LC-MS/MS) analysis of trypsin-digested and chondroitinase ABC-digested HSulf-2 WT led to the identification of a HSulf-2 specific glycopeptide comprising a remnant CS hexasaccharide linked to the S₅₈₃ residue (Figure S5). Noteworthy, analysis also showed the presence of the monosulfated CS hexasaccharide linked to S₅₈₃ of the same peptide, as well as the same peptide without any glycosylation. This clearly highlights a marked diversity of HSulf-2 GAG modification, with a most likely strong structural heterogeneity of the CS/DS chain and the co-existence of GAG-free and GAG-bearing forms. In contrast, HSulf-2ΔSG showed no such glycopeptides.

We also analyzed HSulf-2ΔSG by SEC-MALLS (Figure 2D). As expected, HSulf-2ΔSG eluted significantly later than HSulf-2 WT. However, the detected peak was shouldered, thus suggesting the presence of two species. Furthermore, results obtained for the major species yielded a calculated unexpectedly high MW of 239 ± 30 kDa. In line with this, SAXS analysis confirmed a dramatic reduction in size of HSulf-2ΔSG compared with the WT, with a calculated D_{max} of 24 nm and an MW of ~240 kDa, which supported well our SEC-MALLS data (Figures S1E–S1H).

To understand better the discrepancies between MALDI MS and SAXS/SEC-MALLS MW estimations, we analyzed HSulf-2ΔSG by mass photometry, another biophysical approach that allows accurate mass measurement of proteins in solution, in their native state. The results (Figure 2F) confirmed the presence

of two species in a 1:2 ratio, whose calculated masses matched that of a monomer (137 kDa) for the first species and that of a dimer (283 kDa) for the second and most abundant one. Interestingly, analysis of HSulf-2 WT yielded broad and heterogeneous peaks but also showed one minor and one major species of 157 and 316 kDa, respectively. These could fit monomeric and dimeric forms for HSulf-2 harboring a ~20 kDa GAG chain. However, considering the natural structural diversity of GAG chains, as well as the co-existence of both GAG-free and GAG-bearing HSulf-2 forms (Figure S5), further analysis will be required to investigate a possible dimerization of HSulf-2 WT.

Altogether, these data provide converging evidence that HSulf-2 features an unexpected PTM at the level of its HD domain, corresponding to a covalently linked ~20–25 kDa CS/DS polysaccharide chain. This result thus highlights that HSulf-2 as a member related to the large PG family.

Endogenous expression of GAG-modified HSulf-2

We identified a GAG chain on HSulf-2 when overexpressed in HEK transfected cells. To confirm the physiological relevance of these findings, we sought to demonstrate the presence of this GAG chain on the naturally occurring enzyme. In this attempt, we isolated trypsin-digested and chondroitinase ABC-digested PGs from the culture medium of human neuroblastoma SH-SY5Y cells. Analysis by nano-scale LC-MS/MS analysis led to the identification of an HSulf-2-specific, 21-amino-acid-long glycopeptide, highlighting a consensus CS/DS attachment tetrasaccharide linker on the S₅₈₃ residue of an endogenously expressed HSulf-2 (Figures 3A and 3B).

To obtain further insights into GAG modification of endogenously expressed HSulf-2, we analyzed HSulf-2 expressed by two additional cell types: MCF7 human breast cancer cells and human umbilical vein endothelial cells (HUVECs). Detection and characterization of endogenous Sulfs were challenging. Expression yields are usually low, and WB immunodetection yields different band patterns, depending on cells, PTMs, and furin cleavages (see Figure 1). To address these issues, we made use of Sulf high *N*-glycosylation content and used a protocol of culture medium enrichment based on a lectin affinity chromatography. We analyzed enriched conditioned medium by WB, using antibodies raised against either HSulf-2 N-terminal (H2.3) (Uchimura et al., 2006) or C-terminal (2B4) (Lemjabbar-Alaoui et al., 2010) subunits (Figure 1). WB analysis of HSulf-2 secreted in the conditioned medium of MCF7 using 2B4 yielded broad diffuse bands in the ~66–130 and ~185–270 kDa size range, respectively (Figure 3C, lane 1). We attributed these bands to CS/DS-conjugated C-terminal subunit fragments and to a CS/DS-conjugated full-length, furin-uncleaved HSulf-2 form, respectively. The presence of the CS/DS chain was confirmed by chondroitinase ABC treatment, which converted the broad bands into two sets of well-defined bands, corresponding to a GAG-depolymerized full-length unprocessed form and C-terminal fragments (Figure 3C, lane 2). Although difficult to ascertain, we speculate that the ladder band pattern obtained for the C-terminal subunit could reflect structural heterogeneity within the HD domain, possibly due to furin secondary cleavage (see Figure 1) and/or partial degradation (Tang and Rosen, 2009). However, these changes could definitely be attributed to the

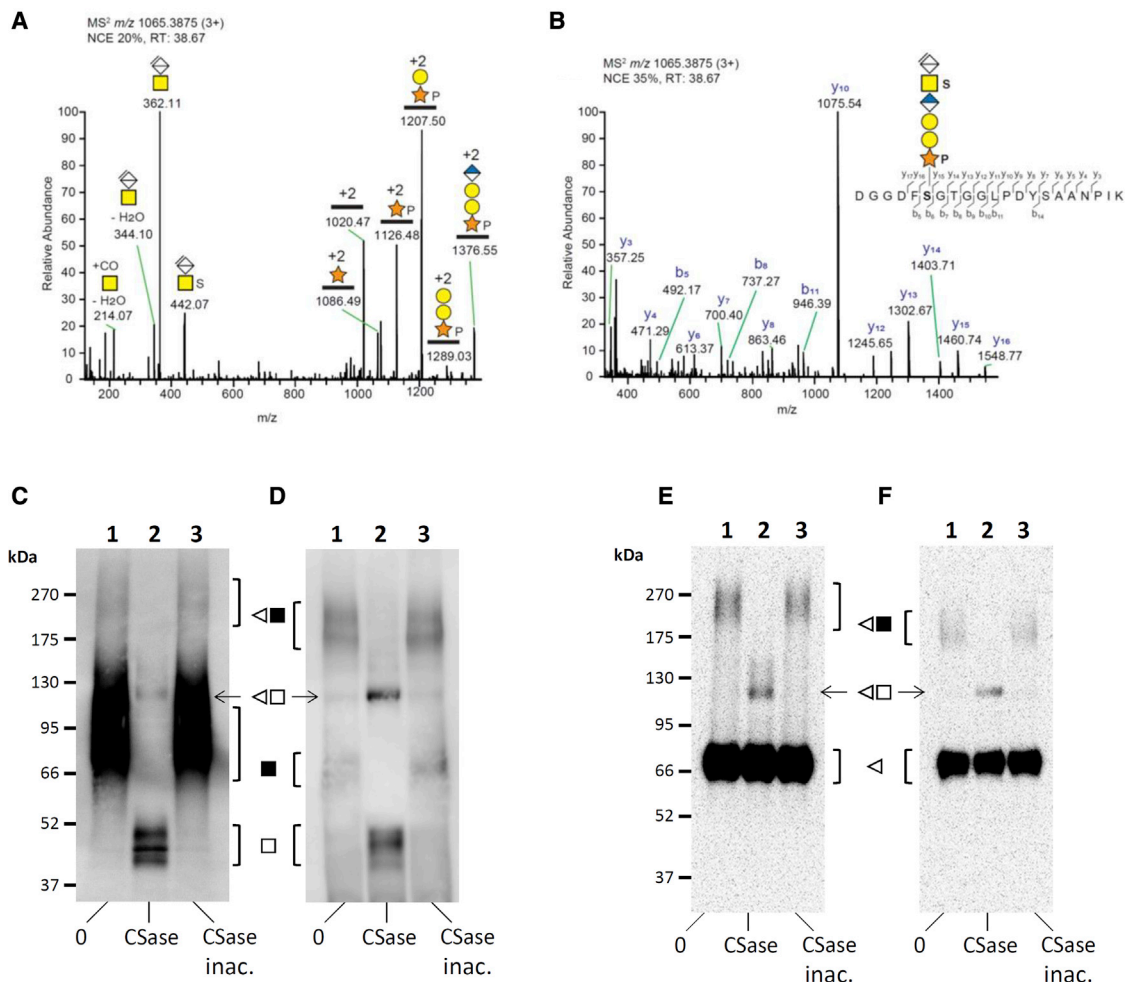


Figure 3. Endogenous expression of GAG-bearing HSulf-2 in SH-SY5Y cells, MCF7 cells, and HUVECs

(A and B) LC-MS/MS detection of a CS/DS GAG linkage region attached to S₅₈₃ of endogenously expressed HSulf-2 by SH-SY5Y cells. HSulf-2 glycopeptides were obtained by trypsin digestion of media of cultured SH-SY5Y cells, followed by enrichment on a SAXS column, and thereafter treatment with chondroitinase ABC. The spectral files were filtered for the MS² diagnostic ion at *m/z* 362.1083 corresponding to the (ΔHexA-HexNAc) disaccharide, common to all CS/DS linkage region glycopeptides. (A) MS² spectrum of the 578-DGGDFSGTGGPLDYSAANPIK-598 glycopeptide obtained by higher-energy collisional dissociation (HCD) with normalized collision energy (NCE) of 20%, providing prominent glycan fragmentations. (B) MS² spectrum of the same glycopeptide obtained at NCE of 35%, displaying peptide sequence fragmentation with b- and y-ions annotated in the sequence. The positioning and distinction of sulfate (79.9568 u) and phosphate (79.9663 u) modifications were done by manually interpreting the MS² spectra. The MS² spectrum thus displayed a mass shift of 79.9570 u between *m/z* 362.1083 and *m/z* 442.0653, demonstrating the presence of a sulfate modification on the GalNAc residue. A mass shift of 212.0084 u was observed between *m/z* 1,019.9724 (2+) and *m/z* 1,125.9766 (2+), demonstrating the presence of a xylose plus phosphate modification of the peptide (the theoretical mass of this modification is 212.0086 u [132.0423 u + 79.9663 u]).

(C–F) Endogenous expression of GAG-bearing HSulf-2 in MCF7 cells and HUVECs. WB analysis of pre-purified concentrated conditioned medium from MCF7 cells (C, E) and HUVECs (D, F) using anti-C-ter 2B4 (C, D) and anti-N-ter H2.3 antibodies (E, F), prior to (0, lanes 1) or after treatment with chondroitinase ABC (CS, lanes 2). Digestions with heat-inactivated chondroitinase ABC were used as controls (CS inac., lanes 3). The nature of detected bands is shown as follows: black symbols for CS/DS-conjugated fragments; white symbols for GAG-free fragments; triangles for the N-terminal subunit; squares for the C-terminal subunit. Of note, analysis indicates the presence in both samples of unprocessed forms (triangle + square, sharp band at ~125 kDa) and, at least in the HUVEC conditioned medium, the presence of GAG-free HSulf-2 forms (bands corresponding to C-ter fragments within the 40–57 kDa MW range, and an unprocessed form at 125 kDa detected in the untreated samples, gel B lanes 1 and 3).

cleavage of the GAG chains, as the treatment with heat-inactivated chondroitinase ABC showed the same band pattern as the non-treated samples (Figure 3C, lane 3).

Analysis of HSulf-2 from HUVEC pre-purified conditioned medium yielded similar results (Figure 3D) but with remarkable differences. First, detected signals were markedly less intense,

especially for the CS/DS modified forms. Although quantification by immunodetection should be cautiously considered, this suggested that expression levels of HSulf-2 and proportions between GAG-free and GAG-bearing forms may be different between MCF7 cells and HUVECs. We also noticed discrepancies regarding furin processing activity (distinct ratios between

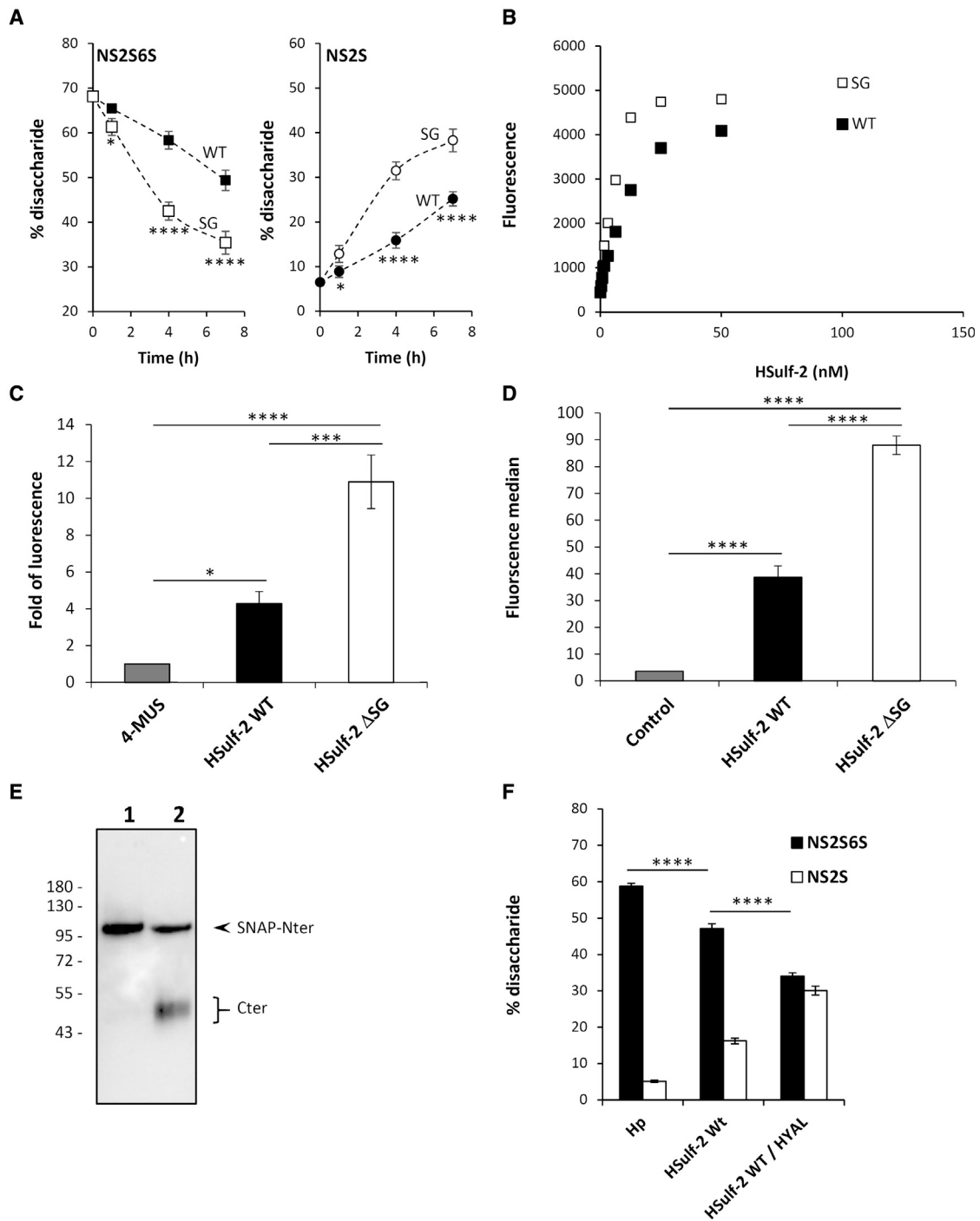


Figure 4. *In vitro* binding and sulfatase activity of HSulf-2 WT and GAG-free HSulf-2

(A) HS 6-O-endosulfatase activity of HSulf-2 WT (n = 3, black symbols) and HSulf-2ΔSG (n = 3, white symbols) was assessed by monitoring the time-course digestion of [UA(2S)-GlcNS(6S)] trisulfated disaccharides (NS2S6S, squares) into [UA(2S)-GlcNS] disulfated disaccharides (NS2S, circles). Data are expressed as a percentage of total disaccharide content. Error bars indicate SD.

(B) Binding immunoassay of HSulf-2 WT (black) and HSulf-2ΔSG (white) to a streptavidin-immobilized heparin surface. Data are representative of three independent experiments.

(C) The aryl-sulfatase activity of HSulf-2 WT (n = 3, black) and HSulf-2ΔSG (n = 3, white) was measured using 4MUS fluorogenic pseudo-substrate. The results are expressed as a fluorescence fold increase compared with negative control (4MUS alone, n = 3, gray).

(D) Binding of HSulf-2 WT (n = 3, black) and HSulf-2ΔSG (n = 3, white) to the surface of human amnion-derived Wish cells was monitored by FACS using the H2.3 anti-HSulf-2 antibody and compared with control (n = 3, gray). Error bars indicate SD.

(legend continued on next page)

processed and unprocessed forms). WB analysis using the N-terminal reactive H2.3 antibody confirmed the presence of the N-terminal subunit being unaffected by the chondroitinase ABC treatment (~75 kDa size), and supported the identification of full-length unprocessed forms within the analyzed samples (~160–250 kDa size range, Figures 3E and 3F). Finally, although WB analysis showed similar band patterns for these two cell lines (Figures 3C and 3D), GAG-conjugated fragments from HUVECs migrated at slightly lower aMW (~60–75 and ~160–250 kDa, lane 1 in Figure 3D versus 3C).

Altogether, these results confirm that endogenously expressed HSulf-2 harbors a CS/DS chain and indicates the co-existence of GAG-modified and GAG-free forms. Furthermore, our data suggest cell-dependent specificities of HSulf-2 PTM (e.g., furin processing and the GAG structure), which could provide additional regulation/diversity of the enzyme's structural and functional features.

HSulf-2 GAG chain modulates enzyme activity *in vitro*

The HD is a major functional domain of the Sulfs. This domain is required for the enzyme's high-affinity binding to HS substrates and for processive 6-O-endosulfatase activity (Frese et al., 2009; Seffouh et al., 2013; Tang and Rosen, 2009). We thus anticipated that the presence of a GAG chain on this domain would significantly affect the enzyme substrate recognition and activity.

To this end, we assessed HSulf-2 WT and HSulf-2ΔSG 6-O-endosulfatase activities, using heparin as a surrogate of HS. We analyzed the disaccharide composition of HSulf-2-treated heparin and measured the content of [UA(2S)-GlcNS(6S)] trisulfated and [UA(2S)-GlcNS] disulfated disaccharides, which are the enzyme's primary substrate and reaction product, respectively (Frese et al., 2009; Pempe et al., 2012; Seffouh et al., 2013). The results (Figure 4A) showed enhanced digestion of the disaccharide substrate with HSulf-2ΔSG versus HSulf-2 WT (time: $F_{3, 16} = 272.7$, $p < 0.0001$; HSulf-2 type: $F_{1, 16} = 140.5$, $p < 0.0001$; interaction: $F_{3, 16} = 28.57$, $p < 0.0001$), and a concomitant increase in the [UA(2S)-GlcNS] disaccharide product at 1 h incubation and thereafter until 7 h (time: $F_{3, 16} = 394$, $p < 0.0001$; HSulf-2 type: $F_{1, 16} = 195$, $p < 0.0001$; interaction: $F_{3, 16} = 39.94$, $p < 0.0001$). We speculated that the observed increase in endosulfatase activity could be due to an improved enzyme-substrate interaction. We thus analyzed the binding of HSulf-2 WT and HSulf-2ΔSG to surface-coated biotinylated heparin. The results showed an increase, albeit modest, in HSulf-2ΔSG binding to heparin, with calculated K_D of 10.2 ± 0.4 nM and 7.1 ± 0.8 nM for HSulf-2 WT and HSulf-2ΔSG, respectively (Figure 4B).

The second functional domain of the Sulfs, CAT, comprises the enzyme active site. CAT alone is unable to catalyze HS 6-O-desulfation, but it exhibits a generic arylsulfatase activity that can be measured using the fluorogenic pseudo-substrate 4-methyl umbelliferyl sulfate (4-MUS). Surprisingly, HSulf-

2ΔSG showed greater (~2.5-fold increase) arylsulfatase activity than that of HSulf-2 WT (Figure 4C, HSulf-2 type: $F_{2, 6} = 90.18$, $p < 0.0001$). We thus concluded from these observations that the CS/DS chain of HSulf-2 regulates the enzyme activity, both by modulating HD domain/substrate interaction and by hindering access to the active site. We hypothesize that these effects could be due to electrostatic hindrance preventing the interaction of the enzyme functional domains with sulfated substrates.

Aside from enzyme activity, the interaction of HS with the Sulf HD domain is also involved in the retention of the enzyme at the cell surface, a mechanism that may also govern diffusion and bioavailability of the enzyme within tissues (Frese et al., 2009). To investigate this, we analyzed the interaction of HSulf-2 WT and HSulf-2ΔSG with cellular HS by fluorescence-activated cell sorting (FACS), using human amniotic epithelial Wish cells as a model. Again, the results showed a significant increase in binding of the HSulf-2 form lacking the CS/DS chain to Wish cells (Figure 4D, HSulf-2 type: $F_{2, 6} = 536.7$, $p < 0.0001$). These data therefore suggest that the HSulf-2 GAG chain may also influence enzyme retention at the cell surface.

As GAG-lacking HSulf-2ΔSG variant exhibited enhanced HS 6-O-endosulfatase activity, we sought to investigate whether enzymatic removal of the HSulf-2 GAG chain would lead to a similar effect. Hyaluronidases are the only mammalian enzymes to exhibit chondroitinase activity (Bilong et al., 2021; Csoka et al., 2001). We found that treatment of HSulf-2 WT with bovine hyaluronidase allowed WB detection of the ~50 kDa band corresponding to the enzyme C-terminal subunit (Figure 4E), and boosted heparin 6-O-desulfation (Figure 4F) with an efficiency similar to that of the HSulf-2ΔSG variant.

HSulf-2 GAG chain modulates tumor growth and metastasis in cultured cells and *in vivo*

We next investigated the effect of HSulf-2 GAG modification on the enzyme pro-oncogenic properties. For this we used MDA-MB-231 cells, a human breast cancer cell line that does not express any HSulfs endogenously (Peterson et al., 2010). As observed on Wish cells, binding of HSulf-2 to MDA-MB-231 cell-surface HS was significantly enhanced for the GAG-lacking HSulf-2ΔSG variant compared with the WT form (Figure 5A, HSulf-2 type: $F_{2, 6} = 26.34$, $p = 0.0011$). We then overexpressed either HSulf-2 WT or HSulf-2ΔSG by lentiviral transduction in MDA-MB-231 cells. After selection, stable expression of Sulfs in transduced cells was confirmed by WB. In contrast, cells transduced with an unrelated protein (dsRed) showed no endogenous expression of the Sulfs (Figure S6A). We also validated the endosulfatase activity of HSulf-2 produced in MDA-MB-231 by treating heparin with concentrated conditioned medium from transduced cells. The results showed no activity for the medium of dsRed-transfected cells while conditioned medium from either HSulf-2 WT or HSulf-2ΔSG transduced cells efficiently digested heparin, as shown by the increase of [UA(2S)-GlcNS]

(E) WB analysis of HSulf-2 WT (lane 1) and hyaluronidase-treated HSulf-2 WT (lane 2), using the anti-HD H19 antibody.

(F) [UA(2S)-GlcNS(6S)] trisulfated disaccharide (NS2S6S, black) and [UA(2S)-GlcNS] disulfated disaccharide (NS2S, white) content (as in A, expressed as a percentage of total disaccharide content, $n = 3$) of heparin, without (Hp) or after digestion with HSulf-2 WT or hyaluronidase (HYAL)-treated HSulf-2 WT (4 h at 37°C). Data show significantly increased heparin 6-O-desulfation for HYAL-treated HSulf-2 WT. Error bars indicate SD.

* $p < 0.05$, ** $p < 0.001$, *** $p < 0.0001$.

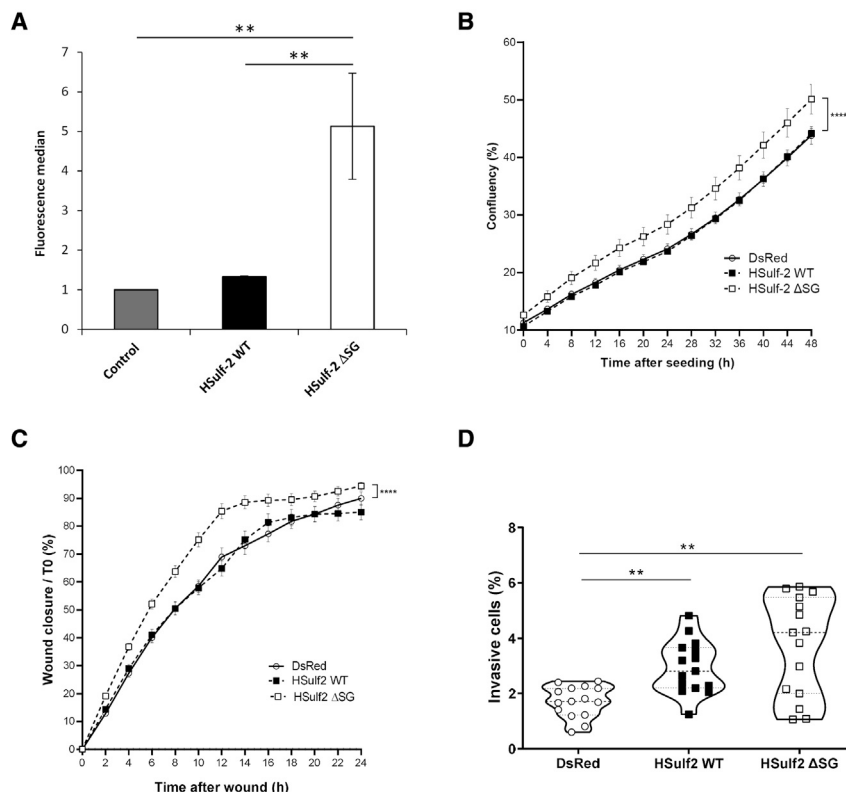


Figure 5. Effects of HSulf-2 WT and HSulf-2ΔSG on the proliferation, migration, and invasion of MDA-MB231 cells

(A) Binding of HSulf-2 WT (n = 3, black) and HSulf-2ΔSG (n = 3, white) to the surface of MDA-MB-231 cells was monitored by FACS using the H2.3 anti-HSulf-2 antibody and compared with control (n = 3, gray). Error bars indicate SD, **p < 0.01.

(B) Cell proliferation was monitored by analyzing the occupied area (% confluency) of cell images over time. dsRed, HSulf-2 WT, or HSulf-2ΔSG transduced MDA-MB-231 cells were imaged every 4 h for 48 h. ****p < 0.001, significantly different from dsRed. Values represent mean ± SEM (n = 68). The experiment shown is representative of three independent experiments.

(C) Quantification of wound closure using the Incucyte S3 software was monitored from images captured at t = 0 and every 2 h for the duration of the experiment. Values represent mean ± SEM (n = 60); ****p < 0.001, significantly different from dsRed. The experiment shown is representative of three independent experiments.

(D) Cell invasion was monitored by counting cells that passed through the Boyden chamber membrane after 24 h. ANOVA Kruskal-Wallis test **p < 0.01 on mean values (n = 15), significantly different from dsRed.

disaccharide product (Figure S6B). Again, the results suggested higher endosulfatase activity for HSulf-2ΔSG transduced cells. Finally, we confirmed the presence of the CS/DS chain on MDA-MB-231 HSulf-2 WT by treating conditioned medium with chondroitinase ABC followed by WB analysis (Figure S6C). Of note, the results also showed a significant proportion of GAG-free and full-length unprocessed forms of HSulf-2 in the chondroitinase ABC-untreated conditioned medium (Figure S6C, lane 1).

MDA-MB-231 cells transduced with either mock, HSulf-2 WT, or HSulf-2ΔSG were then analyzed in proliferation, migration, and invasion assays (Figures 5B–5D). The results showed that expression of HSulf-2ΔSG enhanced both cell proliferation and cell migration while HSulf-2 WT transduced cells showed no significant differences from the control (Figures 5B and 5C). In contrast, expression of both HSulf-2 WT and HSulf-2ΔSG promoted cell invasion when compared with control cells (Figure 5D).

Lastly, we analyzed the effect of the HSulf-2 GAG chain on tumor progression *in vivo* using a mouse xenograft model of tumorigenesis and metastasis. For this, dsRed, HSulf-2 WT, or HSulf-2ΔSG transduced MDA-MB-231 cells were xenografted into the mammary gland of mice with severe combined immunodeficiency (SCID). Tumor volumes were monitored every 2 days, and xenografted SCID mice were euthanized when the first tumors reached 1 cm³ in size (day 52), in accordance with the European ethical rule on animal experimentation. Primary tumors, along with lymph nodes and lungs, were collected for further analysis. The results showed little effect of HSulf-2 WT expres-

sion on the tumor size (Figure 6A). Our data are therefore in disagreement with previous work, which reported either anti-oncogenic (Peterson et al., 2010) or pro-oncogenic (Zhu et al., 2016) effects of HSulf-2 WT expression in MDA-MB-231 cells using similar *in vivo* mouse models. However, it should be noted that a major difference between these three studies is the size of xenografted tumors achieved (~0.04 cm³ and 3–4 cm³ respectively, in the studies mentioned above). Such conflicting data clearly exemplify the complexity of HSulf regulatory functions and possible bias that could result from the experimental design. In contrast, expression of the HSulf-2ΔSG variant significantly promoted tumor growth in comparison with both dsRed and HSulf-2 WT conditions. Noteworthy, WB analysis of tumors confirmed sustained expression of the enzyme in both HSulf-2 WT and HSulf-2ΔSG—but not dsRed—conditions (Figure S6D). Histological analysis of tumor sections using hematoxylin/eosin staining showed greater necrotic area in control tumors than in HSulf-expressing tumors (Figure 6B). As necrosis is a hallmark of hypoxia in growing tumors that is mainly due to lack of angiogenesis, we studied tumor vascularization using α -smooth muscle actin (α SMA) immunostaining. The results showed no apparent changes in α SMA labeling upon HSulf-2 WT expression. However, tumor vascularization was increased in HSulf-2ΔSG tumors (Figures S7A and S7B). We next analyzed lymph nodes and lungs for the presence of secondary tumors. Lung, which is a primary target for metastasis in this tumor model, was affected in all conditions (Figure 6C). However, the size of lung metastasis was significantly greater in HSulf-2ΔSG-expressing tumors (Figures 6D and 6E). Moreover, metastasis could be observed with higher frequency in lateral (left axillary) but also contralateral (right axillary) lymph

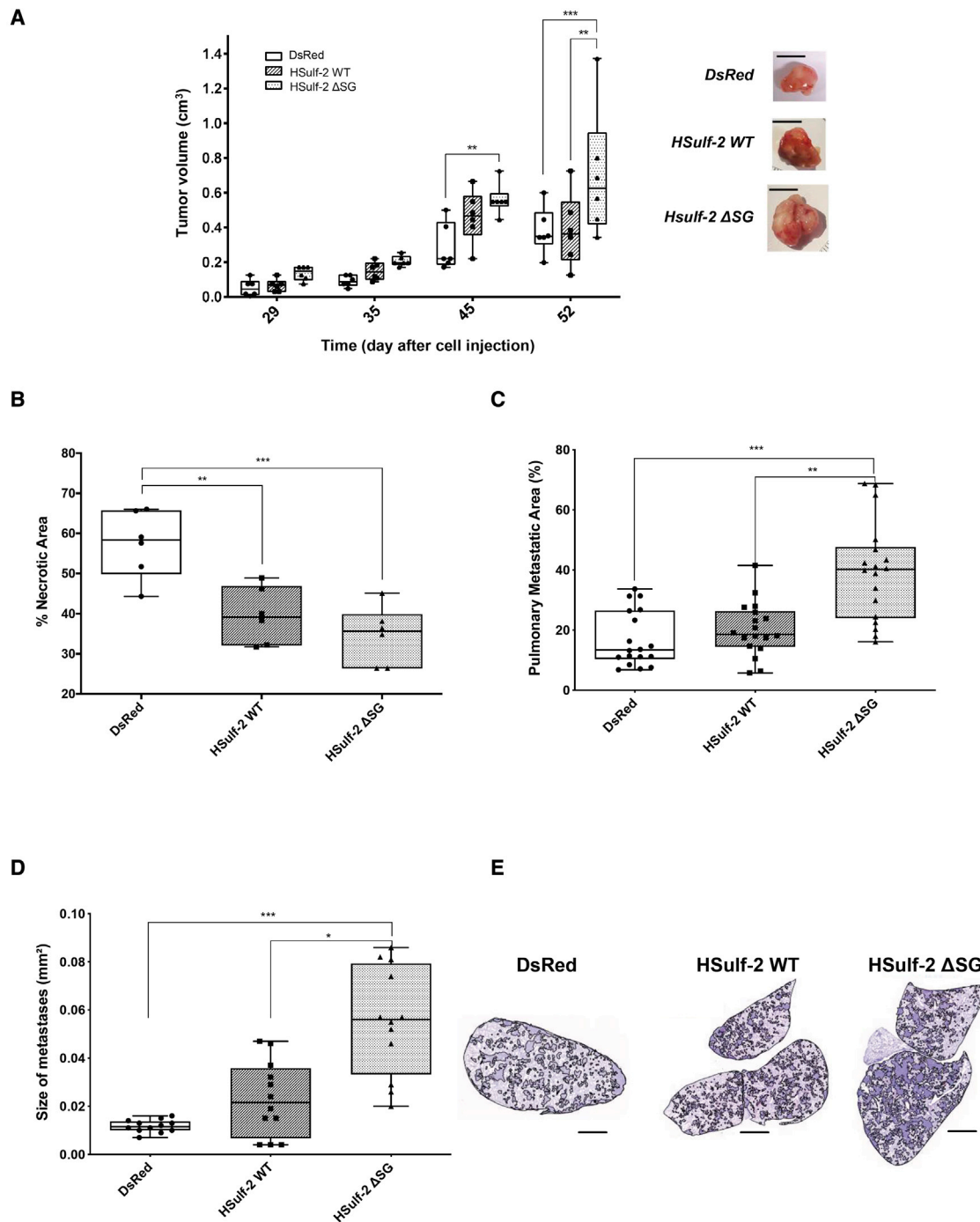


Figure 6. Effects of HSulf-2 WT and HSulf-2ΔSG during tumor progression and metastasis

(A) Time-course measurement of tumor size induced by MDA-MB-231 cells expressing dsRed, HSulf-2 WT, or HSulf-2ΔSG. Statistical analysis was performed using a two-way ANOVA test on mean values, *** $p \leq 0.001$ and ** $p < 0.01$. Pictures representative of each tumor group, at day 52. Scale bars, 1 cm (right panel).

(B) Histological analysis of necrotic area using hematoxylin/eosin (H&E) staining of tumors expressing mock dsRed, HSulf-2 WT, and HSulf-2ΔSG. The percentage of necrotic area was determined on three sections from each of the six mice in each group (one-way ANOVA test, multiple comparison on mean values, Tukey's test, $n = 6$; *** $p \leq 0.001$ and ** $p < 0.01$).

(C) Histological analysis of the percentage of pulmonary metastatic area from dsRed, HSulf-2, and HSulf-2ΔSG-expressing tumors. The measurement was performed on three sections from each of the six mice in each group (one-way ANOVA test, multiple comparison on mean values, Tukey's test, $n = 18$; ** $p < 0.01$ and *** $p < 0.001$).

(D) The size of pulmonary metastasis in each group was quantified and analyzed as in (C) ($n = 12$, ** $p < 0.05$ and *** $p < 0.001$).

(E) Representative images of H&E-stained sections of indicated lung. Scale bars, 1 mm.

nodes for HSulf-2-expressing tumors (Figure S8C). The CS/DS chain borne by HSulf-2 is thus functionally relevant *in vivo*, at least in the context of cancer, where it attenuated the effect of the enzyme on tumor growth and metastatic invasion. In contrast, forms of HSulf-2 lacking the CS/DS chain stimulate the metastatic properties of cancer cells, thus highlighting the importance of HSulf-2 GAG modification status for considering the enzyme as a potential therapeutic target for treating human cancer.

DISCUSSION

In this study, we first showed that extracellular sulfatase HSulf-2 harbors a covalently linked CS/DS chain. A first indication of this was brought to light during the purification of the protein, which featured an abnormally high aMW in SEC. As SEC co-purification of GAG-protein tight complexes is not unusual, we carefully analyzed the protein using different biophysical approaches to demonstrate the covalent nature of this interaction (Figure 2). Converging evidence supporting our conclusion include: (1) an extremely high MW calculated by SEC-MALLS, SAXS, and mass photometry; (2) a dramatic reduction of the MW following chondroitinase ABC digestion, or treatment of the HSulf-2-expressing cells with xylosides; (3) the incapacity of high NaCl concentrations to dissociate, even partially, the HSulf-2/GAG complex; (4) the direct identification of an S₅₈₃-linked CS glycopeptide by MS analysis of trypsin/chondroitinase ABC-digested HSulf-2 WT; and (5) the effect of a single Ser to Ala amino acid mutation on a putative GAG attachment site that resumes the expected behavior of the protein in SEC/SEC-MALLS/SAXS. It should be noted that MW determination for HSulf-2 WT showed significant variations according to the method used. On the contrary, results were much more consistent for the HSulf-2ΔSG variant, thus underlining the tremendous heterogeneity provided by the GAG chain. Most interestingly, these latter data revealed that HSulf-2ΔSG is mostly present as a dimer. Mass photometry analysis also showed a similar distribution for the WT form. However, this could be again the result of GAG structural diversity along with the co-existence of GAG-free and GAG-bearing forms. Further investigations will be needed to clarify the structural basis and functional relevance of the HSulf-2 dimerization state.

Although CS/DS chains have been previously identified on the mucin-like domain of ADAMTS (Mead et al., 2018), the identification of HSulf-2 as a secreted PG-related enzyme is unforeseen. It is well established that GAG chains provide most of PG's biological activities, usually through the ability of the polysaccharide to bind and modulate a wide array of structural and signaling proteins. However, we show here that the GAG chain present on HSulf-2 directly modulates its enzyme activity. These findings open unexpected perspectives in the understanding of the enzyme's biological functions and should contribute to clarify discrepancies in the literature. Here, we first demonstrated that the CS/DS chain modulates HSulf-2 6-O-endosulfatase activity *in vitro*, and we located this GAG chain attachment site in the HD domain of HSulf-2, which is critical for substrate binding. We therefore speculate that this CS/DS chain may tune the HSulf-2 activity, most likely by competing with sulfated sub-

strates for HS binding site occupancy, and/or through electrostatic hindrance. It should be emphasized that our *in vitro* enzyme assays were performed using heparin as a substrate, which is significantly more sulfated than naturally occurring HS and may thus easily outcompete the HSulf-2 CS/DS chain for access to the substrate-binding site. Differences in activity between HSulf-2 WT and the HSulf-2ΔSG may therefore have been largely underestimated. In support of this, binding of HSulf-2ΔSG on surface-coated highly sulfated heparin was only moderately increased compared with the WT, whereas differences were very marked on naturally occurring less sulfated HS of Wish and MDA-MB-231 cell surfaces.

We next analyzed the effect of the HSulf-2 GAG chain in various cell assays and in an *in vivo* mouse xenograft model of cancer. Our data showed that overexpression of the HSulf-2ΔSG variant with increased *in vitro* activity promoted significantly cell proliferation, migration, and invasion (Figure 5). Accordingly, HSulf-2ΔSG also enhanced tumor growth, vascularization, and metastasis in our *in vivo* assay (Figure 6). Although these data clearly highlight that the HSulf-2 GAG chain acts as a modulator of the enzyme pro-tumoral activity, the underlying mechanism has yet to be clarified. First, aside from tuning enzyme/substrate binding, we anticipate that the HSulf-2 GAG chain could also modulate the enzyme function through other mechanisms in an *in vivo* biological context. GAGs bind a wide array of cell-surface and extracellular matrix proteins. The HSulf-2 CS/DS chain could therefore promote the recruitment of GAG-binding proteins, with potentially significant functional consequences. These interactions may involve HSulf-2 in the regulation of matricrine signaling activities or influence the diffusion and distribution of the enzyme within tissues. In line with this, our FACS-based cell-binding assay suggested enhanced attachment to the cell surface of the HSulf-2ΔSG variant versus the HSulf-2 WT form. Consequently, *in vivo* HSulf-2 "GAGosylation" status may not only influence the extent of HS 6-O-desulfation but also the range of the enzyme activity and access to specific HS subsets in tissues. It should also be noted that both our cell and *in vivo* assays only provide information on cell-autonomous effects of HSulf-2. SCID mice used in this study are immunocompromised and may therefore not provide a true extracellular environment for the tumor xenograft. As HSulf-2 is a secreted enzyme, it may also influence tumor progression by acting on cells present in the tumor microenvironment, such as cancer-associated fibroblasts, endothelial cells, or immune cells, among others. Further studies will be needed to evaluate this with the use of other relevant *in vivo* models such as syngeneic models or patient-derived xenografts on humanized mice. Noteworthy, we found that the HSulf-2ΔSG variant had pro-metastatic properties in our *in vivo* assay. The development of metastasis is a multi-step process, which is a major factor of poor prognosis in cancer. Although the biological mechanisms that drive metastasis are relatively unknown, the role of cancer cell-derived matrix proteins as pro-metastatic has been recently highlighted (Tian et al., 2020). Our data therefore further suggest that HSulf-2 also participates in the extracellular matrix remodeling process, and could provide an additional target to act on metastasis development. Moreover, HSulf-2 GAGosylation status could also serve as a metastatic promoting marker.

Beyond the field of cancer, this concept of GAGosylation status should prove to be critical for studying the biological functions of the Sulfs, as this may confer to the enzyme a tremendous level of structural heterogeneity and, therefore, functional diversity. It is first well known that the structure and binding properties of GAGs vary according to the biological context. We therefore anticipate further regulation of HSulf-2 catalytic activity and/or diffusion properties depending on structural features of its CS/DS chain. In addition, our data highlighted differences in HSulf-2 furin processing among analyzed cell types. This could be functionally relevant, as furin maturation may affect HSulf-2 cell surface/extracellular localization as well as *in vivo* activity (Tang and Rosen, 2009). As GAGs have been previously shown to promote furin activity (Pasquato et al., 2007), we could thus hypothesize that the presence of HSulf-2 CS/DS chain at the vicinity of the two major furin cleavage sites may also influence HSulf-2 maturation status.

Here, we succeeded in detecting the endogenous expression by WB of HSulf-2 in MCF7 cells and HUVECs. Because of the signal heterogeneity yielded by the enzyme C-terminal domains, interpretation of the data was challenging. However, results indicated the presence of a GAG chain on endogenously expressed HSulf-2. Furthermore, they suggest that both GAG-conjugated and GAG-free HSulf-2 co-exist depending on the cell type, as WB analysis of GAG-conjugated HSulf-2 fragments from MCF7 cells and HUVECs yielded distinctly different band patterns (Figure 3). The balance of expression between these two forms may therefore be critical for the control of the HS 6-O-desulfation process. The underlying mechanisms are likely to be complex and multi-factorial. Interestingly, we showed that bovine hyaluronidases could efficiently digest the HSulf-2 GAG chain and enhance its endosulfatase activity (Figures 4E and 4F). Mammalian hyaluronidases are a family of six enzymes that catalyze the degradation of hyaluronic acid and also exhibit the ability to depolymerize CS (Csoka et al., 2001; Jedrzejas and Stern, 2005; Kaneiwa et al., 2010). Hyaluronidase expression is increased in some cancers (McAtee et al., 2014), with suggested roles in tumor invasion and tumor-associated inflammation (Dominguez-Gutierrez et al., 2021; McAtee et al., 2014). However, their precise contribution remains poorly understood and contradictory. Here, we propose another function for these enzymes, which may provide an activating mechanism of HSulf-2, through their ability to “unleash” the enzyme from its GAG chain. This perspective urges us to investigate in detail the interplay of HSulf-2 and hyaluronidases during tumor progression as well as in other physiopathological conditions. In line with this, we have analyzed in detail the molecular features of the HSulf-2 GAG chain and the effects of hyaluronidase on its structure and activity (I.S. et al., unpublished data).

Last but not least, analysis of the other human isoform HSulf-1 showed an absence of any GAG chain, at least in our HEK293 overexpressing system (Figure S2G). GAGosylation status could thus account for the functional differences reported between these two secreted endosulfatases.

In conclusion, we report here a most unexpected PTM of HSulf-2 by identifying the presence of a CS/DS chain on the enzyme. Our data highlight this GAG chain as a non-catalytic regulatory element of HSulf-2 activity, which may change per-

spectives in the study of this highly intriguing enzyme and complex regulatory mechanism of HS biological functions. Finally, it is worth noting that such a structurally and functionally relevant feature as a GAG chain on HSulf-2 has remained overlooked for more than 20 years. Beyond the field of the Sulfs, our findings therefore strongly encourage reconsidering afresh the importance of PTMs in complex enzymatic systems.

Limitations of the study

In this study, we have shown that extracellular sulfatase HSulf-2 harbors a covalently linked CS/DS chain and that this chain modulates the enzyme activity. There are, however, a number of limitations to this study that should be emphasized.

Although we showed that the HSulf-2 GAG chain affects enzyme activity *in vitro*, in cell functional assays, and *in vivo*, our study does not provide precise insights into the underlying mechanisms. Whether the observed effects are exclusively linked to the modulation of enzyme activity remains to be clarified. The HSulf-2 GAG chain may also modulate enzyme diffusion and/or sequestration at the cell surface or within the extracellular matrix and elicit interactions with other yet unidentified GAG-binding partners.

Here, we highlighted the need to consider the GAGosylation status of HSulf-2 for future investigations of its biological functions. We have also shown that a subset of cell-expressed HSulf-2 does not carry any GAG chain, which suggests that the ratio of GAG-bearing/GAG-free HSulf-2 may change according to cells and tissues. Likewise, the structural features of HSulf-2 CS/DS chain may also be cell-/tissue-dependent, with consequences on its protein-binding properties and activities. Therefore, we anticipate that the observed biological effects of HSulf-2 GAGosylation may vary significantly according to the biological system considered.

STAR★METHODS

Detailed methods are provided in the online version of this paper and include the following:

- KEY RESOURCES TABLE
- RESOURCE AVAILABILITY
 - Lead contact
 - Materials availability
 - Data and code availability
- EXPERIMENTAL MODEL AND SUBJECT DETAILS
 - Cell lines
 - Mouse model
- METHOD DETAILS
 - Antibodies against HSulf-2
 - Production and purification of recombinant WT and mutant HSulf-2
 - Analysis of HSulf-2 expression
 - SEC-MALLS analysis
 - SAXS analysis
 - Mass photometry analysis
 - MALDI-TOF MS analysis of HSulf-2ΔSG
 - LC-MS/MS identification of HSulf-2 GAG chain and its attachment site

- *In vitro* enzyme activity assays
- Analysis of HSulf-2/heparin binding immuno-assay
- FACS analysis
- Lentiviral transduction of MDA-MB 231 cells
- Proliferation assay
- Wound-healing migration assay
- Matrigel invasion assay
- *In vivo* experiments

● **QUANTIFICATION AND STATISTICAL ANALYSIS**

SUPPLEMENTAL INFORMATION

Supplemental information can be found online at <https://doi.org/10.1016/j.celrep.2022.110516>.

ACKNOWLEDGMENTS

The authors would like to thank the animal unit staff (I. Jeannin, S. Bama, C. Magallon, N. Chaumontel, and H. Pointu) at the Interdisciplinary Research Institute of Grenoble (IRIG) for animal husbandry, Rabia Sadir for her help with mass photometry, and Caroline Mas of the ISBG biophysical platform. This work used the platforms of the Grenoble Instruct-ERIC center (ISBG; UMS 3518 CNRS-CEA-UJF-EMBL) within the Grenoble Partnership for Structural Biology. Platform access was supported by FRISBI (ANR-10-INBS-05-02) and GRAL, a project of the Université Grenoble Alpes graduate school (Ecoles Universitaires de Recherche) CBH-EUR-GS (ANR-17-EURE-0003). This work was also supported by the CNRS and the GDR GAG (GDR 3739), the “Investissements d’avenir” program Glyco@Alps (ANR-15-IDEX-02), by grants from the Agence Nationale de la Recherche (ANR-12-BSV8-0023, ANR-17-CE11-0040, and ANR-19-CE13-0031) and Université Grenoble Alpes (UGA AGIR program), the Swedish Research Council (2017-00955 to G.L. and to the Swedish National Infrastructure for Biological Mass Spectrometry), and the Ingabritt and Arne Lundbergs Forskningsstiftelse. IBS (Institut de Biologie Structurale) acknowledges integration into the IRIG (CEA).

AUTHOR CONTRIBUTIONS

R.E.M. and A.S. performed most of the biochemical experiments, with additional contributions from E.G., F.D., M.F.-A., and Y.C. C.R. and R.E.M. performed cellular and *in vivo* experiments and data processing under the supervision of O.F. J.P. performed SAXS analysis and modeling. K.N. and K.U. performed biochemical analysis of HSulf-2 endogenous expression. All glycoproteomics LC-MS/MS analyses were prepared, performed, and interpreted by F.N., M.N., and G.L. in collaboration with the BIOMS proteomics core facility at the University of Gothenburg. R.D. and I.S. performed MS analysis. R.R.V., O.F., and H.L.-J. interpreted the data and supervised experimental work. R.R.V., R.E.M., K.U., and O.F. wrote the manuscript with the help of all co-authors.

DECLARATION OF INTERESTS

The authors declare no competing interests.

Received: January 25, 2021

Revised: October 7, 2021

Accepted: February 17, 2022

Published: March 15, 2022

REFERENCES

Ai, X., Do, A.T., Kusche-Gullberg, M., Lindahl, U., Lu, K., and Emerson, C.P., Jr. (2006). Substrate specificity and domain functions of extracellular heparan sulfate 6-O-endosulfatases, QSulf1 and QSulf2. *J. Biol. Chem.* *281*, 4969–4976.

Ambasta, R.K., Ai, X., and Emerson, C.P., Jr. (2007). Quail Sulf1 function requires asparagine-linked glycosylation. *J. Biol. Chem.* *282*, 34492–34499.

Bilong, M., Bayat, P., Bourderieux, M., Jérôme, M., Giuliani, A., and Daniel, R. (2021). Mammal hyaluronidase activity on chondroitin sulfate and dermatan sulfate: mass spectrometry analysis of oligosaccharide products. *Glycobiology* *31*, 751–761.

Bret, C., Moreaux, J., Schved, J.F., Hose, D., and Klein, B. (2011). SULFs in human neoplasia: implication as progression and prognosis factors. *J. Transl. Med.* *9*, 72.

Chua, J.S., and Kuberan, B. (2017). Synthetic xylosides: probing the glycosaminoglycan biosynthetic machinery for biomedical applications. *Acc. Chem. Res.* *50*, 2693–2705.

Csoka, A.B., Frost, G.I., and Stern, R. (2001). The six hyaluronidase-like genes in the human and mouse genomes. *Matrix Biol.* *20*, 499–508.

Dhoot, G.K., Gustafsson, M.K., Ai, X., Sun, W., Standiford, D.M., and Emerson, C.P., Jr. (2001). Regulation of Wnt signaling and embryo patterning by an extracellular sulfatase. *Science* *293*, 1663–1666.

Dierks, T., Dickmanns, A., Preusser-Kunze, A., Schmidt, B., Mariappan, M., von Figura, K., Ficner, R., and Rudolph, M.G. (2005). Molecular basis for multiple sulfatase deficiency and mechanism for formylglycine generation of the human formylglycine-generating enzyme. *Cell* *121*, 541–552.

Dominguez-Gutierrez, P.R., Kwenda, E.P., Donelan, W., O’Malley, P., Crispin, P.L., and Kusmartsev, S. (2021). Hyal2 expression in tumor-associated myeloid cells mediates cancer-related inflammation in bladder cancer. *Cancer Res.* *81*, 648–657.

El Masri, R., Seffouh, A., Lortat-Jacob, H., and Vivès, R.R. (2017). The “in and out” of glucosamine 6-O-sulfation: the 6th sense of heparan sulfate. *Glycoconj. J.* *34*, 285–298.

Esko, J.D., and Zhang, L. (1996). Influence of core protein sequence on glycosaminoglycan assembly. *Curr. Opin. Struct. Biol.* *6*, 663–670.

Frese, M.A., Milz, F., Dick, M., Lamanna, W.C., and Dierks, T. (2009). Characterization of the human sulfatase Sulf1 and its high affinity heparin/heparan sulfate interaction domain. *J. Biol. Chem.* *284*, 28033–28044.

Hanson, S.R., Best, M.D., and Wong, C.H. (2004). Sulfatases: structure, mechanism, biological activity, inhibition, and synthetic utility. *Angew. Chem. Int. Ed. Engl.* *43*, 5736–5763.

Harder, A., Möller, A.-K., Milz, F., Neuhaus, P., Walhorn, V., Dierks, T., and Anselmetti, D. (2015). Catch bond interaction between cell-surface sulfatase Sulf1 and glycosaminoglycans. *Biophys. J.* *108*, 1709–1717.

Henriet, E., Jäger, S., Tran, C., Bastien, P., Michelet, J.-F., Minondo, A.-M., Formanek, F., Dalko-Csiba, M., Lortat-Jacob, H., Breton, L., et al. (2017). A jasmonic acid derivative improves skin healing and induces changes in proteoglycan expression and glycosaminoglycan structure. *Biochim. Biophys. Acta* *1861*, 2250–2260.

Jedrzejak, M.J., and Stern, R. (2005). Structures of vertebrate hyaluronidases and their unique enzymatic mechanism of hydrolysis. *Proteins Struct. Funct. Bioinforma.* *61*, 227–238.

Kaneiwa, T., Mizumoto, S., Sugahara, K., and Yamada, S. (2010). Identification of human hyaluronidase-4 as a novel chondroitin sulfate hydrolase that preferentially cleaves the galactosaminidic linkage in the trisulfated tetrasaccharide sequence. *Glycobiology* *20*, 300–309.

Konarev, P.V., Volkov, V.V., Sokolova, A.V., Koch, M.H.J., and Svergun, D.I. (2003). PRIMUS: a Windows PC-based system for small-angle scattering data analysis. *J. Appl. Crystallogr.* *36*, 1277–1282.

Lemjabbar-Alaoui, H., van Zante, A., Singer, M.S., Xue, Q., Wang, Y.Q., Tsay, D., He, B., Jablons, D.M., and Rosen, S.D. (2010). Sulf-2, a heparan sulfate endosulfatase, promotes human lung carcinogenesis. *Oncogene* *29*, 635–646.

Li, J.-P., and Kusche-Gullberg, M. (2016). Heparan sulfate: biosynthesis, structure, and function. *Int. Rev. Cell Mol. Biol.* *325*, 215–273.

McAtee, C.O., Barycki, J.J., and Simpson, M.A. (2014). Emerging roles for hyaluronidase in cancer metastasis and therapy. *Adv. Cancer Res.* *123*, 1–34.

Mead, T.J., McCulloch, D.R., Ho, J.C., Du, Y., Adams, S.M., Birk, D.E., and Apte, S.S. (2018). The metalloproteinase-proteoglycans ADAMTS7 and ADAMTS12 provide an innate, tendon-specific protective mechanism against heterotopic ossification. *JCI Insight* *3*, e92941.

- Morimoto-Tomita, M., Uchimura, K., Werb, Z., Hemmerich, S., and Rosen, S.D. (2002). Cloning and characterization of two extracellular heparin-degrading endosulfatases in mice and humans. *J. Biol. Chem.* *277*, 49175–49185.
- Noborn, F., Gomez Toledo, A., Sihlbom, C., Lengqvist, J., Fries, E., Kjellen, L., Nilsson, J., and Larson, G. (2015). Identification of chondroitin sulfate linkage region glycopeptides reveals prohormones as a novel class of proteoglycans. *Mol. Cell. Proteomics* *14*, 41–49.
- Noborn, F., Nikpour, M., Persson, A., Sihlbom, C., Nilsson, J., and Larson, G. (2022). A Glycoproteomic Approach to Identify Novel Proteoglycans. *Methods Mol Biol* *2303*, 71–85.
- Paquato, A., Dettin, M., Basak, A., Gambaretto, R., Tonin, L., Seidah, N.G., and Di Bello, C. (2007). Heparin enhances the furin cleavage of HIV-1 gp160 peptides. *FEBS Lett.* *581*, 5807–5813.
- Pempe, E.H., Burch, T.C., Law, C.J., and Liu, J. (2012). Substrate specificity of 6-O-endosulfatase (Sulf-2) and its implications in synthesizing anticoagulant heparan sulfate. *Glycobiology* *22*, 1353–1362.
- Pérard, J., Nader, S., Levert, M., Arnaud, L., Carpentier, P., Siebert, C., Blanquet, F., Cavazza, C., Renesto, P., Schneider, D., et al. (2018). Structural and functional studies of the metalloregulator Fur identify a promoter-binding mechanism and its role in *Francisella tularensis* virulence. *Commun. Biol.* *1*, 93.
- Peterson, S.M., Iskenderian, A., Cook, L., Romashko, A., Tobin, K., Jones, M., Norton, A., Gomez-Yafal, A., Heartlein, M.W., Concino, M.F., et al. (2010). Human Sulfatase 2 inhibits in vivo tumor growth of MDA-MB-231 human breast cancer xenografts. *BMC Cancer* *10*, 427.
- Petoukhov, M.V., Franke, D., Shkumatov, A.V., Tria, G., Kikhney, A.G., Gajda, M., Gorba, C., Mertens, H.D.T., Konarev, P.V., and Svergun, D.I. (2012). New developments in the ATSAS program package for small-angle scattering data analysis. *J. Appl. Crystallogr.* *45*, 342–350.
- Rosen, S.D., and Lemjabbar-Alaoui, H. (2010). Sulf-2: an extracellular modulator of cell signaling and a cancer target candidate. *Expert Opin. Ther. Targets* *14*, 935–949.
- Sarrazin, S., Lamanna, W.C., and Esko, J.D. (2011). Heparan sulfate proteoglycans. *Cold Spring Harb Perspect. Biol.* *3*, a004952.
- Seffouh, A., Milz, F., Przybylski, C., Laguri, C., Oosterhof, A., Bourcier, S., Sadr, R., Dutkowski, E., Daniel, R., van Kuppevelt, T.H., et al. (2013). HSulf sulfatases catalyze processive and oriented 6-O-desulfation of heparan sulfate that differentially regulates fibroblast growth factor activity. *Faseb. J.* *27*, 2431–2439.
- Seffouh, A., El Masri, R., Makshakova, O., Gout, E., Hassoun, Z.E.O., Andrieu, J.-P., Lortat-Jacob, H., and Vivès, R.R. (2019a). Expression and purification of recombinant extracellular sulfatase HSulf-2 allows deciphering of enzyme sub-domain coordinated role for the binding and 6-O-desulfation of heparan sulfate. *Cell. Mol. Life Sci.* *76*, 1807–1819.
- Seffouh, I., Przybylski, C., Seffouh, A., El Masri, R., Vivès, R.R., Gonnet, F., and Daniel, R. (2019b). Mass spectrometry analysis of the human endosulfatase HSulf-2. *Biochem. Biophys. Rep.* *18*, 100617.
- Svergun, D.I. (1992). Determination of the regularization parameter in indirect-transform methods using perceptual criteria. *J. Appl. Crystallogr.* *25*, 495–503.
- Tang, R., and Rosen, S.D. (2009). Functional consequences of the subdomain organization of the sulfs. *J. Biol. Chem.* *284*, 21505–21514.
- Tian, C., Öhlund, D., Rickelt, S., Lidström, T., Huang, Y., Hao, L., Zhao, R.T., Franklin, O., Bhatia, S.N., Tuveson, D.A., et al. (2020). Cancer cell-derived matrix proteins promote metastasis in pancreatic ductal adenocarcinoma. *Cancer Res.* *80*, 1461–1474.
- Uchimura, K., Morimoto-Tomita, M., Bistrup, A., Li, J., Lyon, M., Gallagher, J., Werb, Z., and Rosen, S.D. (2006). HSulf-2, an extracellular endoglucosamine-6-sulfatase, selectively mobilizes heparin-bound growth factors and chemokines: effects on VEGF, FGF-1, and SDF-1. *BMC Biochem.* *7*, 2.
- Vives, R.R., Seffouh, A., and Lortat-Jacob, H. (2014). Post-synthetic regulation of HS structure: the Yin and Yang of the sulfs in cancer. *Front. Oncol.* *3*, 331.
- Walhorn, V., Möller, A.-K., Bartz, C., Dierks, T., and Anselmetti, D. (2018). Exploring the sulfatase 1 catch bond free energy landscape using jarzynski's equality. *Sci. Rep.* *8*, 16849.
- Yang, J.D., Sun, Z., Hu, C., Lai, J., Dove, R., Nakamura, I., Lee, J.S., Thorgeirsson, S.S., Kang, K.J., Chu, I.S., et al. (2011). Sulfatase 1 and sulfatase 2 in hepatocellular carcinoma: associated signaling pathways, tumor phenotypes, and survival. *Genes Chromosomes Cancer* *50*, 122–135.
- Zhu, C., He, L., Zhou, X., Nie, X., and Gu, Y. (2016). Sulfatase 2 promotes breast cancer progression through regulating some tumor-related factors. *Oncol. Rep.* *35*, 1318–1328.

STAR★METHODS

KEY RESOURCES TABLE

REAGENT or RESOURCE	SOURCE	IDENTIFIER
Antibodies		
Rabbit polyclonal anti-HSulf-2 antibody	Biotem (Apprieu)	H19
Rabbit anti HSulf-2 C-terminal subunit antibody	R&D Systems	Mab7087; RRID:AB_10971958
Rabbit anti HSulf-2 N-terminal subunit antibody	(Uchimura et al., 2006)	H2.3
Rabbit Anti α SMA	Abcam	Ab124964; RRID:AB_11129103
Antigen Unmasking Solution	Vector Laboratories	Cat #H-3300
Bacterial and virus strains		
BL21/DE3 E. coli	NEB	Cat #C2527
Chemicals, peptides, and recombinant proteins		
4-Methylumbelliferyl sulfate potassium salt (4-MUS)	Sigma-Aldrich	M7133
RIPA buffer	Sigma-Aldrich	R0278
Bovine hyaluronidase	Sigma-Aldrich	H3506
TBA	Sigma-Aldrich	155837
2-cyano acetamide	Sigma-Aldrich	108448
Matrigel Growth Factor Reduced Basement Membrane Matrix	Corning/ Becton Dickinson	Cat #354230
Formaldehyde (4% Paraformaldehyde)	Sigma-Aldrich	Cat #HT5011
Hoechst 33258	Sigma-Aldrich	Cat #94403
Puromycin	Sigma-Aldrich	Cat #P8833
Polybrene	Sigma-Aldrich	Cat #H9268
Mitomycin C	Sigma-Aldrich	Cat #M5353
Heparinases I	GrampEnz	GE-H0001
Heparinases II	GrampEnz	GE-H0002
Heparinases III	GrampEnz	GE-H0003
HS disaccharide standard 001	Iduron	HD001
HS disaccharide standards 002	Iduron	HD002
HS disaccharide standards 003	Iduron	HD003
HS disaccharide standards 004	Iduron	HD004
HS disaccharide standards 005	Iduron	HD005
HS disaccharide standards 006	Iduron	HD006
HS disaccharide standards 007	Iduron	HD007
HS disaccharide standards 008	Iduron	HD008
Critical commercial assays		
Substrate kit, peroxidase Vector NovaRED	Vector Laboratories	Cat #SK-4800
Histostain™-Plus 3rd Gen IHC Detection Kit	Invitrogen	Cat #859073
Micro BCA protein Assay kit	Thermo Scientific	Cat #23235
Deposited data		
MS Data Figures 3 and S5	PRIDE	PXD031408
MS Data Figure S4	MassIVE	MSV000088782
Experimental models: Cell lines		
FreeStyle HEK293 cells	ThermoFisher	R79007
MDA-MB-231 cells	ATCC	Cat#HTB-26
MCF-7 cells	Japanese Collection of Research Bioresources Cell Bank	JCRB0134

(Continued on next page)

Continued		
REAGENT or RESOURCE	SOURCE	IDENTIFIER
HUVEC cells	Japanese Collection of Research Bioresources Cell Bank	IFO50271
Wish cells	ATCC	CCL-25
Experimental models: Organisms/strains		
Immunodeficient NOD/Scid/ γ C (NSG) mice	The Jackson Laboratory via Charles River	Cat #005557
Recombinant DNA		
HSulf-2 (WT)	Addgene	(#13004)
HSulf-2 variants	This paper	N/A
Plasmid pLVX-DsRed N1	Clontech	Cat #32560
pSPAX2	Addgene	Cat ##12260
pCMV-VSV-G	Addgene	Cat ##8454
Software and algorithms		
PRIMUS software for SAXS analysis	(Konarev et al., 2003)	PRIMUS
GNOM software for SAXS analysis	(Svergun, 1992)	GNOM
Fiji quantification software	https://imagej.net/software/fiji/	Fiji
FlexAnalysis MS software	https://bruker-daltonics-flexanalysis.software.informer.com	Bruker Daltonics flexAnalysis 3.3.80.0
IncuCyte Zoom	Sartorius	https://uol.de/fileadmin/user_upload/fzns/download/STED/Documents/IncuCyte_R_S3_-_Live-Cell_Imaging_and_Analysis__AR_PDF.pdf
Other		
Agilent 1200 series HPLC	Agilent Technologies	https://www.agilent.com/en/products/liquid-chromatography
SEC-MALLS	Wyatt -Hitachi	https://www.isbg.fr/biophysics-characterisation/sec-malls/?lang=en
Mass photometry	Reyfen One MP	https://www.isbg.fr/biophysics-characterisation/mass-photometer-one/

RESOURCE AVAILABILITY

Lead contact

Further information and requests for resources and reagents should be directed to and will be fulfilled by the lead contact, Romain R. Vivès (romain.vives@ibs.fr).

Materials availability

This study did not generate new unique reagents.

Data and code availability

- Mass spectrometry data have been deposited at PRIDE and MassIVE and are publicly available as of the date of publication. Accession numbers are listed in the [key resources table](#). All data reported in this paper will be shared by the lead contact upon request.
- This paper does not report original code.
- Any additional information required to reanalyze the data reported in this paper is available from the lead contact upon request.

EXPERIMENTAL MODEL AND SUBJECT DETAILS

Cell lines

FreeStyle HEK293 cells (ThermoFisher scientific, ref R79007) were used for recombinant protein production. Cells were grown in Freestyle medium (Thermo fisher scientific) under agitation, at 37°C, in a 5% CO₂-95% air atmosphere.

MDA-MB-231 cells (ATCC, ref Cat#HTB-26) were cultured in Leibovitz's medium (Life Technologies) supplemented with 10% fetal bovine serum, 100 U/mL of penicillin, 100 µg/mL of streptomycin (Life Technologies), at 37°C, in a 5% CO₂–95% air atmosphere.

MCF-7 cells were obtained from the Japanese Collection of Research Bioresources Cell Bank (Osaka, Japan) and maintained in Dulbecco's Modified Eagle Medium (Life Technologies) supplemented with 10% fetal bovine serum (Biowest, Nuaille, France), 100 U/mL of penicillin, and 100 µg/mL of streptomycin (Life Technologies), at 37°C, in a 5% CO₂–95% air atmosphere.

HUVEC cells were obtained from the Japanese Collection of Research Bioresources Cell Bank (IFO50271) and maintained in Endothelial Cell Growth Medium 2 (PromoCell, Heidelberg, Germany) supplemented with 2% fetal bovine serum, Growth Medium 2 Supplement Mix (PromoCell), 100 U/mL of penicillin, and 100 µg/mL of streptomycin, at 37°C, in a 5% CO₂–95% air atmosphere.

Wish cells (ATCC, ref CCL-25) were maintained in Dulbecco's Modified Eagle Medium (Life Technologies) supplemented with 10% fetal bovine serum (Biowest, Nuaille, France), 100 U/mL of penicillin, and 100 µg/mL of streptomycin (Life Technologies), at 37°C, in a 5% CO₂–95% air atmosphere.

Mouse model

7-weeks-old female NOD SCID GAMMA/J mice were purchased from Charles River and maintained in the Animal Resources Center of our department. *In vivo* experiment protocols were approved by the institutional guidelines and the European Community for the Use of Experimental Animals.

METHOD DETAILS

Antibodies against HSulf-2

The epitopes of antibodies against HSulf-2 are summarized in [Figure 1](#). Polyclonal antibody H19 was newly produced by Biotem (Apprieu, France), by immunizing rabbits with a mix of 2 peptides derived from HSulf-2 sequence (C₅₀₆DSGDYKLSLAGRRKKLF and T₅₆₃KRHWPAPEDQDDKDG), located with the HD domain, on each side of the furin cleavage sites (see [Figure 1](#)). Consequently, H19 is specific of the HD domain and recognizes both HSulf-2 N- and C-terminal subunits. The 2B4 monoclonal antibody, which is specific of HSulf-2 C-terminal subunit, was purchased from R&D Systems (Mab7087). Of note, analysis of whole lysates prepared from cultured cells or tissues with 2B4 yields a sharp ~130 kDa band. This band presumably corresponds to a form in synthesis, such as non furin-processed/GAG-unmodified HSulf-2. Meanwhile, analysis of conditioned medium with 2B4 shows multiple bands corresponding to HSulf-2 unmodified or Furin/GAG-modified C-terminal subunit. The H2.3 polyclonal antibody, which is specific to the HSulf-2 N-terminal subunit, was previously described ([Uchimura et al., 2006](#)).

Production and purification of recombinant WT and mutant HSulf-2

The expression and purification of HSulf-2 and mutants were performed as described previously ([Seffouh et al., 2019a](#)). Briefly, FreeStyle HEK293 cells (Thermo fisher scientific) were transfected with pcDNA3.1 vector encoding for HSulf-2 cDNA flanked by TEV cleavable SNAP (20.5 kDa) and His tags at N- and C-terminus, respectively. The protein was purified from conditioned medium by cation exchange chromatography on an SP Sepharose column (GE healthcare) in 50 mM Tris, 5 mM MgCl₂, 5 mM CaCl₂, pH 7.5, using a 0.1–1 M NaCl gradient, followed by size exclusion chromatography (Superdex200, GE healthcare) in 50 mM Tris, 300 mM NaCl, 5 mM MgCl₂, 5 mM CaCl₂, pH 7.5. Treatment of HSulf-2 with chondroitinase ABC was achieved by incubating 250 µg of enzyme with 100mU chondroitinase ABC (Sigma) overnight at 4°C. HSulf-2ΔSG mutants (ΔSG, ΔSG1, ΔSG2) were generated by site directed mutagenesis (ISBG Robiomol platform) and purified as above.

Analysis of HSulf-2 expression

MDA-MB-231 cells were lysed with RIPA buffer for 2 h at 4°C and tissues were disrupted and lysed in RIPA buffer (Sigma-Aldrich) using a MagNA Lyser instrument (Roche) with ceramic beads. Supernatants were collected and protein concentration was determined using a BCA protein Assay kit (Thermo Scientific). Cell lysates (eq. of 3 × 10⁵ cells), tumor lysates (eq. of 50 µg of total proteins) or purified recombinant proteins were then separated by SDS-PAGE, followed by transfer onto PVDF membrane. Proteins were probed using either rabbit polyclonal H19 (dil. 1/1000) or mouse monoclonal 2B4 (dil. 1/500) antibodies, followed by incubation with HRP-conjugated anti-rabbit (Thermo Scientific, dil. 1/5000), anti-mouse (Thermo Scientific, dil. 1/5000) secondary antibodies.

Endogenous CS/DS modification of HSulf-2 was analyzed in two cell lines: the MCF-7 human breast cancer cells and human umbilical vein endothelial cells (HUVECs). MCF-7 cells were cultured at 37°C for 48 h in OPTI-MEM, after which culture medium was collected and concentrated on Amicon Ultra Filters (30 kDa cut-off, Millipore, Burlington, MA). Conditioned medium from MDA-MB231 cells was prepared likewise, using FreeStyle medium instead of OPTI-MEM. HSulf-2 in concentrated samples was analyzed by Western blotting as described below. HUVECs were cultured at 37°C in OPTI-MEM containing 0.5% FBS for 24 h, after which culture medium was collected and concentrated on Amicon Ultra Filters. Concentrated samples were incubated with GlcNAc-binding wheat germ agglutinin (WGA)-coated beads (Vector Laboratories, Burlingame, CA) at 4°C overnight, and proteins that were captured by WGA beads were analyzed by Western blotting. For elimination of CS/DS chains, the concentrated MCF-7 culture media or WGA bead-bound materials were treated with chondroitinase ABC (1 U/mL) or heat-inactivated chondroitinase ABC (1 U/mL), at 37°C for 1 h. Proteins in the samples were separated by SDS-PAGE with 5–20% gels (Wako Pure Chemical Industries, Osaka, Japan)

and were transferred to PVDF membranes. HSulf-2 proteins were probed with the 2B4 mouse monoclonal anti-HSulf-2 antibody (dil. 1/500) or the H2.3 rabbit polyclonal anti-HSulf-2 antibody (dil. 1/500) followed by a horseradish peroxidase-labeled anti-mouse or rabbit IgG antibody (Cell Signaling Technology, Danvers, MA) and ImmunoStar LD (Wako Pure Chemical Industries). Signals were visualized by using a LuminoGraph image analyzer (ATTO, Tokyo, Japan).

SEC-MALLS analysis

SEC-MALLS analysis was performed using a Superose 6 Increase 10/300GL size-exclusion chromatography column (GE healthcare) equilibrated in 50 mM Tris, 300 mM NaCl, 5 mM MgCl₂, 5 mM CaCl₂, pH 7.5 at 0.5 mL/min, coupled to an L-2400 UV detector (Hitachi), an Optilab T-rEX refractometer (Wyatt technologies) and a DAWN HELEOS-II multi angle light scattering detector (Wyatt technologies). Protein concentration was quantified online by measuring the differential refractive index and using an averaged refractive index increment dn/dc of 0.185 mL/g. Accurate weight-averaged molar masses (MW) determination was performed with the Astra 6 software (Wyatt Technologies).

SAXS analysis

SAXS data were collected at the European Synchrotron Radiation Facility (Grenoble, France) on the BM29 beamline at BioSAXS. The standard energy as set to 12.5 keV and a Pilatus 1M detector was used to record the scattering patterns. The sample-to-detector distance was set to 2.867 m (q-range is 0.025–6 nm⁻¹). Samples were set in quartz glass capillary with an automated sample changer. The scattering curve of the buffer (before and after) solution was subtracted from the sample's SAXS curves. Scattering profiles were measured at several concentrations, from 0.5 to 1.5 mg/mL at room temperature. Data were processed using standard procedures with the ATSAS v2.8.3 suite of programs (Petoukhov et al., 2012). The *ab initio* determination of the molecular shape of the proteins was performed as previously described (Pérard et al., 2018). Radius of gyration (Rg) and forward intensity at zero angle (I(0)) were determined with the programs PRIMUS (Konarev et al., 2003), by using the Guinier approximation at low Q value, in a Q.Rg range <1.5:

$$\ln I(Q) = \ln I(0) - \frac{R_g^2 Q^2}{3}$$

Porod volumes and Kratky plot were determined using the Guinier approximation and the PRIMUS programs. The pairwise distance distribution function P(r) were calculated by indirect Fourier transform with the program GNOM (Svergun, 1992). The maximum dimension (Dmax) value was adjusted in order that the Rg R value obtained from GNOM agreed with that obtained from Guinier analysis.

Mass photometry analysis

Mass Photometry experiments were acquired using a Refeyn OneMP (Refeyn Ltd., Oxford, UK) MP system. AcquireMP and DiscoverMP softwares were used to record movies and analyze data respectively using standard settings. Microscope coverslips (high precision glass coverslips, Marienfeld) were cleaned following Refeyn Ltd. individual rinsing procedure. To keep the sample droplet in shape, reusable self-adhesive silicone culture wells (Grace Bio-Labs reusable CultureWell™ gaskets) were used. Contrast-to-mass calibration was achieved using a mix of proteins with molecular weight of 66, 146, 480 and 1048 kDa in 50 mM Tris, 300 mM NaCl, 5 mM MgCl₂, 5 mM CaCl₂, pH 7.5. Samples drops were formed by adding 1 to 2 μL of protein solution into 18 to 19 μL of buffer, to reach a drop volume of 20 μL and a final protein concentration of 40–60 nM.

MALDI-TOF MS analysis of HSulf-2ΔSG

MS experiments were carried out on a MALDI Autoflex speed TOF/TOF MS instrument (Bruker Daltonics, Germany), equipped with a SmartBeam II™ laser pulsed at 1 kHz. The spectra were recorded in the positive linear mode (delay: 600 ns; ion source 1 (IS1) voltage: 19.0 kV; ion source 2 (IS2) voltage: 16.6 kV; lens voltage: 9.5 kV). MALDI data acquisition was carried out in the mass range 5000–150000 Da, and 10000 shots were summed for each spectrum. Mass spectra were processed using FlexAnalysis software (version 3.3.80.0, Bruker Daltonics). The instrument was calibrated using mono- and multi-charged ions of BSA (BSA Calibration Standard Kit, AB SCIEX, France). HSulf-2ΔSG was desalted as previously described (Seffouh et al., 2019b). MALDI-TOF MS analysis was achieved by mixing 1.5 μL of sinapinic acid matrix at 20 mg/mL in acetonitrile/water (50/50; v/v), 0.1% TFA, with 1.5 μL of the desalted protein solution (0.57 mg/mL).

LC-MS/MS identification of HSulf-2 GAG chain and its attachment site

The glycoproteomics protocol used for characterizing proteoglycans has been published earlier (Noborn et al., 2015) and most recently summarized in detail for analyses of CS proteoglycans of human cerebrospinal fluid (Noborn et al., 2022). In the present work, the starting material was purified, recombinant HSulf-2 WT and HSulf-2ΔSG overexpressed in HEK293 cells. Additionally, we analyzed with the same technique conditioned cell media, without fetal calf serum, obtained from SH-SY5Y cells kindly provided by Drs. Thomas Daugbjerg-Madsen and Katrine Schjoldager, University of Copenhagen, Denmark.

In vitro enzyme activity assays

Detailed protocols for arylsulfatase and endosulfatase assays have been described elsewhere (Seffouh et al., 2019a). For the arylsulfatase assay, we used 4-MUS, a routinely used arylsulfatase non-fluorescent substrate, which converted into fluorescent 4-MU upon loss of its sulfate moiety. Here, the enzyme (2 μ g) was incubated for 4 h with 10 mM 4-MUS (Sigma) in 50 mM Tris, 10 mM MgCl₂ pH 7.5 for 1–4 h at 37°C, and the reaction was followed by fluorescence monitoring (excitation 360 nm, emission 465 nm). Results are expressed as a fold of fluorescence increase compared to negative control (4-MUS alone) and corresponds to means \pm SD of three independent experiments. The endosulfatase assay was achieved by incubating 25 μ g of Heparin with 3 μ g of enzymes in 50 mM Tris, 2.5 mM MgCl₂ pH 7.5, for 4 h at 37°C. Disaccharide composition of Sulf-treated heparin was then determined by exhaustive digestion of the polysaccharide (48 hours at 37°C) with a cocktail of heparinase I, II and III (10 mU each), followed by RPIP-HPLC analysis (Henriet et al., 2017), using NaCl Gradients calibrated with authentic standards (Iduron). HSulf-2 (2 μ g) digestion with bovine hyaluronidase (Sigma/Aldrich, 2 μ g) was achieved after a 2 h incubation in 50 mM Tris pH 7.5 at 37°C, prior to the endosulfatase assay, which was performed as above. Incubation of heparin with bovine hyaluronidase alone showed no effect on the disaccharide analysis (data not shown).

Analysis of HSulf-2/heparin binding immuno-assay

As reported before (Seffouh et al., 2019a), microliter plates were first coated with 10 μ g/mL streptavidin in TBS buffer, then incubated with 10 μ g/mL biotinylated heparin, and saturated with 2% BSA. All the incubations were achieved for 1 h at RT, in 50 mM Tris-Cl, 150 mM NaCl, pH 7.5 (TBS) buffer. Next, the recombinant protein was added, then probed with H2.3 primary rabbit polyclonal anti-HSulf-2 antibody (dil. 1/1000) followed by fluorescent-conjugated secondary anti-rabbit antibody (Jackson ImmunoResearch Laboratories, dil. 1/500). All the incubations were performed for 2 h at 4°C in TBS, 0.05% Tween, and were separated by extensive washes with TBS, 0.05% Tween. Finally, fluorescence of each well was measured (excitation 485 nm, emission 535 nm). K_Ds were determined by Scatchard analysis of the binding data. Results shown are representative of three independent experiments.

FACS analysis

Cells (1 million for each condition) were washed with PBS, 1% BSA (the same buffer is used all along the experiment), and incubated with 5 μ g of HSulf-2 enzymes (2 h at 4°C). After extensive washing, cells were incubated with H2.3 primary antibody (dil. 1/500, 1 h at 4°C), washed again, then with secondary Alexa 488-conjugated antibody (Jackson ImmunoResearch Laboratories, dil. 1/500, 1 h at 4°C). FACS analysis of cell fluorescence was performed on a MACSQuant Analyzer (Miltenyi Biotec, excitation 485 nm, emission 535 nm) by calculating median over 25000 events. Data are represented as means \pm SD of three independent experiments.

Lentiviral transduction of MDA-MB 231 cells

HSulf-2 (WT and variant) encoding cDNAs were cloned into the pLVX lentiviral vector (Clontech). This vector was then used in combination with viral vectors GAG POL (psPAX2) and ENV VSV-G (pCMV) to transduce HEK293T and produce lentiviruses released in the extracellular medium. The pLVX-Ds-Red N1 (Clontech) was used as negative control.

For infection, MDA-MB-231 cells were plated into 6 well-plates (8 x 10⁵ in 2 mL of serum-supplemented Leibovitz's medium). The day after, adherent cells were incubated with 1 mL of lentiviral medium diluted in 1 mL of serum-supplemented medium containing 8 μ g/ μ L of polybrene (Sigma/Aldrich). After 4 h, 1 mL of medium were added to cultures and transduction was maintained for 16 h before washing the cells and changing the medium. For stable transduction, puromycin selection was started 36 h post-infection (at the concentration of 2 μ g/mL, Life Technologies) and was maintained thereafter.

Proliferation assay

MDA-MB-231 cells were seeded in flat bottom 96-well plates (Corning, Falcon, 10 000 cells/well) and incubated at 37°C in a 5% CO₂-95% air atmosphere until confluence. Cells were tracked (one image every 4 h) using an automated live-cell imager with high-throughput capabilities and built-in data analysis (Essen IncuCyte Zoom live-cell microscopy system). Cell proliferation was monitored by analyzing the occupied area (% confluence) of cell images over time.

Wound-healing migration assay

MDA-MB231 cells were seeded in flat bottom 96-well plates (Corning, Falcon, 80 000 cells/well) and incubated until confluence. The cell monolayer was scratched using the Essen Bioscience WoundMaker to create scratch-wounds of a standardized width (~600 μ m) and the wound-healing process was pursued in the presence of growth medium containing the cell proliferation inhibitor mitomycin (5 μ g/mL). Cells were tracked (one image every 2 h) using an automated live-cell imager with high-throughput capabilities and built-in data analysis (Essen IncuCyte Zoom live-cell microscopy system). Image analyses and determinations of wound confluence were performed using the IncuCyte S3 software. Experiments were conducted at 37°C in a 5% CO₂-95% air atmosphere.

Matrigel invasion assay

MDA-MB-231 cells in growth medium supplemented with 0.5% serum were seeded in the upper chamber of the transwell inserts containing Matrigel™ (24-well plate; 8 μ m pore size; Becton Dickinson, 20 000 cells/well). Culture medium containing 10% serum was added to the lower chamber as chemoattractant. After incubation for 24 h at 37°C, cells that did not invade through the pores

were removed using a cotton swab. Invading cells were stained with Hoechst 33258 (Sigma-Aldrich) and nuclei were counted using ImageJ. Results are represented as a percentage of invasive cells.

In vivo experiments

In vivo experiment protocols were approved by the institutional guidelines and the European Community for the Use of Experimental Animals and were conducted on 7-weeks-old female NOD SCID GAMMA/J mice (Charles River). 1×10^6 MDA-MB-231 cells resuspended in 50% MatrigelTM (Becton Dickinson) in Leibovitz medium (Life Technologies) were injected into the fat pad of #4 left mammary gland. Tumor growth was recorded by sequential determination of tumor volume using caliper. Tumor volume was calculated according to the formula $V = ab^2/2$ (a, length; b, width). Mice were euthanized after 52 days through cervical dislocation. Tumors and axillary lymph nodes were collected, weighed and either fixed for 2h in 4% paraformaldehyde (PFA) and embedded in paraffin, or stored at -80°C for WB analysis. Tissue necrosis was assessed by Hematoxylin/eosin staining and ImageJ quantification. For vascularization analysis, sections (5 μm thick) of formalin-fixed, paraffin embedded tumor tissue samples were dewaxed, rehydrated and subjected to antigen retrieval in citrate buffer (Antigen Unmasking Solution, Vector Laboratories) with heat. Slides were incubated for 10 min in hydrogen peroxide H_2O_2 to block endogenous peroxidases and then 30 min in saturation solution (Histostain, Invitrogen) to block non-specific antibody binding. This was followed by overnight incubation, at 4°C , with primary antibody against αSMA (Ab124964, Abcam, dil. 1/500). After washing, sections were incubated with a suitable biotinylated secondary antibody (Histostain kit, Invitrogen) for 10 min. Antigen-antibody complexes were visualized by applying a streptavidin-biotin complex (Histostain, Invitrogen) for 10 min followed by NovaRED substrate (Vector Laboratories). Sections were counterstained with hematoxylin to visualize nucleus. Control sections were incubated with secondary antibody alone. Lungs were inflated using 4% PFA and embedded in paraffin. The metastatic burden was assessed by serial sectioning of the entire lungs, every 200 μm . Hematoxylin and eosin staining was performed on lung and lymph nodes sections (5 μm thick). Images were acquired using AxioScan Z1 (Zeiss) slide scanner and quantified using Fiji software.

QUANTIFICATION AND STATISTICAL ANALYSIS

Experimental data are shown as mean \pm standard error of the mean (SEM) unless specified otherwise. Comparisons between multiple groups were carried out by a repeated-measures two-way analysis of variance (ANOVA) with Tukey's multiple comparisons test (Figure 6A) to evaluate the significance of differential tumor growth between three groups of mice; an ordinary two-way ANOVA with Bonferroni's (Figure 4A) or Sidak's tests (Figures 5B and 5C) and an ordinary one-way ANOVA (Figures 4C, 4D, 5A, 5D, and 6B–6D) were carried out to evaluate *in vitro* activity and binding of HSulf-2, the differential level of necrosis and vascularization inside tumors, and pulmonary metastases (number and area). Prism 8 (GraphPad Software, Inc., CA) was used for analyses. Probability value of less than 0.05 was considered to be significant. * $p < 0.05$, ** $p < 0.01$, *** $p < 0.001$ and **** $p < 0.0001$. Additional statistical details of experiments can be found in the figure legends.